Dalton Transactions

ARTICLE

Mononuclear ruthenium compounds bearing N-donor and N-heterocyclic carbene ligands: structure and oxidative catalysis

Received 00th January 20xx,
Accepted 00th January 20xx

DOI: 10.1039/x0xx00000x

www.rsc.org/

H.-J. Liu,[a] M. Gil-Sepulcre,[a] L. Francàs,[b] R. Bofill,*[a] P. Nolis,[c] T. Parella,[c] J. Benet-Buchholz,[b] X. Fontrodona,[d] Antoni Llobet,[a,b] L. Escriche*[a] and X. Sala*[a]

SINO POSES EL NOM SENCER DESPRES A SCI-FINDER ES MES DIFICIL TROBAR-TE

A new CNNC carbene-phthalazine tetradentate ligand has been synthesized, which under reaction with $[Ru(T)Cl_3]$ (T = trpy, tpm, bpea; trpy = 2,2';6',2"-terpyridine; tpm = tris(pyrazol-1-yl)methane; bpea = N,N-bis(pyridin-2-ylmethyl)ethanamine) in MeOH or iPrOH undergoes a C-N bond scission due to the nucleophilic attack of a solvent molecule, with the subsequent formation of the mononuclear complexes *cis*-$[Ru(PhthaPz\text{-}OR)(trpy)X]^{n+}$, $[Ru(PhthaPz\text{-}OMe)(tpm)X]^{n+}$ and *trans,fac*-$[Ru(PhthaPz\text{-}OMe)(bpea)X]^{n+}$ (X = Cl, n = 1; X = H_2O, n = 2; PhthaPz-OR = 1-(4-alcoxyphthalazin-1-yl)-3-methyl-1H-imidazol-3-ium), named $\mathbf{1a}^{+}/\mathbf{2a}^{2+}$ (R = Me), $\mathbf{1b}^{+}/\mathbf{2b}^{2+}$ (R = iPr), $\mathbf{3}^{+}/\mathbf{4}^{2+}$ and $\mathbf{5}^{+}/\mathbf{6}^{2+}$, respectively. Interestingly, regulation of the stability regions of the different Ru oxidation states is obtained by the different ligand combinations, going from $\mathbf{6}^{2+}$, where Ru(III) is clearly stable and mono-electronic transfers are favoured, to $\mathbf{2a}^{2+}/\mathbf{2b}^{2+}$, where Ru(III) is almost unstable with regards to its disproportion. The catalytic performance of the Ru-OH_2 complexes in chemical water oxidation at pH 1.0 points to poor stability (ligand oxidation), with subsequent evolution of CO_2 together with O_2, specially for $\mathbf{4}^{2+}$ and $\mathbf{6}^{2+}$. In electrochemically driven water oxidation, higher TOF values are obtained for $\mathbf{2a}^{2+}$ at pH 1.0. In alkene epoxidation, complexes favouring bi-electronic transfer processes show better performance and selectivity than those favouring mono-electronic transfers, while alkenes containing electron-donor groups promote better performance than those bearing electron-withdrawers. Finally, when *cis*-β-methylstyrene is employed as substrate, no *cis*/*trans* isomerization takes place, thus indicating the existence of an stereospecific process.

Introduction

N-heterocyclic carbenes (NHCs) are ~~carbenes~~ -neutral compounds featuring a divalent C atom with six electrons in its valence shell- contained within an N-heterocycle that are excellent ligands for transition metal ions (M), forming rather strong M-C bonds and often stable complexes under ambient conditions.[1] AQUESTA FRASE TAN LLARGA EM COSTA DE LLEGIR, JO LA PARTIRIA EN DUES.

Transition metal complexes containing NHCs have found multiple applications in important catalytic transformations, such as hydrogenation, transfer hydrogenation, water reduction and water oxidation.[2]

When designing catalysts for redox processes, controlling the oxidative power and the accessibility and stability of the oxidation states involved in the catalytic cycle is of paramount importance for the selectivity of the catalysed PEL DALTON JO TREURIA AMERICANISMES IS HO DEIAXARIA TO UK - reaction. In general, in the presence of electron-donating ligands (such as carbenes) high oxidation states of the central metal ion will be stabilized, and hence its redox potentials

[a] Departament de Química, Facultat de Ciències, Universitat Autònoma de Barcelona, Cerdanyola del Vallès, 08193 Barcelona (Catalonia), Spain. E-mail: roger.bofill@uab.cat, lluis.escriche@uab.cat, xavier.sala@uab.cat: Fax: + 34 93 581 24 77

[b] Institute of Chemical Research of Catalonia (ICIQ), Av. Països Catalans 16, 43007 Tarragona (Catalonia), Spain.

[c] Servei de Ressonància Magnètica Nuclear, Facultat de Ciències, Universitat Autònoma de Barcelona, Cerdanyola del Vallès, 08193 Barcelona (Catalonia), Spain.

[d] Serveis Tècnics de Recerca, Edifici P-II, Campus Montilivi, Universitat de Girona, 17071 Girona (Catalonia), Spain.

† Electronic Supporting Information (ESI) available: Spectroscopic (NMR, UV-Vis), spectrometric (ESI-MS), electrochemical (CV, DPV, bulk electrolysis, Pourbaix diagrams), catalytic (manometries) and structural (X-Ray diffraction) data. See DOI: 10.1039/x0xx00000x

decrease,[3] thus facilitating oxidative catalytic processes. Additionally, when a water molecule is directly coordinated to the metal centre, the redox properties of the complex will be affected by proton exchange. The successive $1e^-$ oxidations taking place are accompanied by a sequential loss of protons favoured by the enhanced acidity of the bonded aqua ligand. This phenomenon, known as proton coupled electron transfer (PCET), allows transition metals to achieve high oxidation states quite easily, since the successive loss of protons -going from the aqua to the hydroxo and finally oxo ligand- allows the maintenance of the total charge of the complex.[4] In addition ~~Plus,~~ the σ and π donation of the oxo ligand present at high oxidation state further stabilizes high oxidation states at the metal centre. Thus, promising examples in water oxidation catalysis have been reported within the last 6 years with Ir[5] and Ru[6] NHC complexes, most of which are monometallic, although a few ones are multimetallic. Interestingly, during the past years researchers have emphasized the distinctive and sometimes superior performance of bimetallic catalysts because of the possible cooperative interactions existing between both M-OH_2 active sites thanks to their relative disposition imposed by the bridging ligand.[7]

Also, Ru NHC complexes have also found relevant applications in alkene epoxidation catalysis.[8] A remarkable example is the use of Ru-aqua complexes with increasing number NHC units that stabilize the Ru(IV)/Ru(III) redox potential to a much higher extend than the Ru(III)/Ru(II) and thus favouring the disproportion of the Ru(III) oxidation state. As a consequence of this the Ru(IV)=O species becomes a powerful two-electron oxidant. This is interesting because it avoids radical reaction pathways associated with 1 electron oxidation processes.[9] This is particularly interesting for the olefin epoxidation reactions since it will favour a concerted pathway that will generate a stereoselective product.[8]

Within this context, and given the feasible preparation of thermodinamically stable NHCs and the interest in using them as ligands in oxidative catalytic systems, we have synthesized and characterized a new tetradentate NHC ligand (1,4-bis(1-methylimidazolium-1-yl)phthalazine; **L1**$^{2+}$). This new ligand loses a carbine moiety upon reacting with Ru precursors generating the new carbine ligand 3-methyl-1-(phthalazin-1-yl)-1H-imidazol-3-ium) **L2**$^{+}$ and 3-siopropyl-1-(phthalazin-1-yl)-1H-imidazol-3-ium) **L3**$^{+}$ (see Chart 1).

and evaluated its effect on the electrochemical properties and oxidative catalytic activity of the corresponding Ru-aqua complexes. Aixo no ho heu fet perque es trenca abans no?

. Additional auxiliary ligands include: the meridional tridentate N-donor ligand trpy, the facial tri-N-dentate ligand tpm and the either meridional or facial ~~one~~ bpea (trpy = 2,2':6',2''-terpyridine, tpm = tris(pyrazol-1-yl)methane, bpea = N,N-bis(pyridin-2-ylmethyl)ethanamine); Chart 1). Due to the instability of **L1**$^{2+}$ under the synthetic conditions employed, we have obtained the mononuclear complexes *cis*-[Ru(Me-L2)(trpy)X]$^{n+}$, *cis*-[Ru(iPr-L2)(trpy)X]$^{n+}$, [Ru(Me-L2)(tpm)X]$^{n+}$ and *trans,fac*-[Ru(Me-L2)(bpea)X]$^{n+}$ (X = Cl, n = 1, **1**$^{a+}$; X = H_2O, n = 2, **2a**$^{2+}$;

Un pel enrabassat

PhthaPz = 3-methyl-1-(phthalazin-1-yl)-1H-imidazol-3-ium), named, respectively, **1a**$^{+}$/**2a**$^{2+}$, **1b**$^{+}$/**2b**$^{2+}$, **3**$^{+}$/**4**$^{2+}$ and **5**$^{+}$/**6**$^{2+}$, which show interesting redox properties when employed in water oxidation and alkene epoxidation catalysis.

A MI AQUI MI FALTA EL LLIGAND MES IMPORTANT DE TOT EL PAPER EL L2+ I L3+! PER LA NOMEMENCLATURA DELS COMPLEXES ES MOLT FARRAGOS AMB EL NOM COMPLET. L'ABREUJAMENT HO FAS MES FACIL.

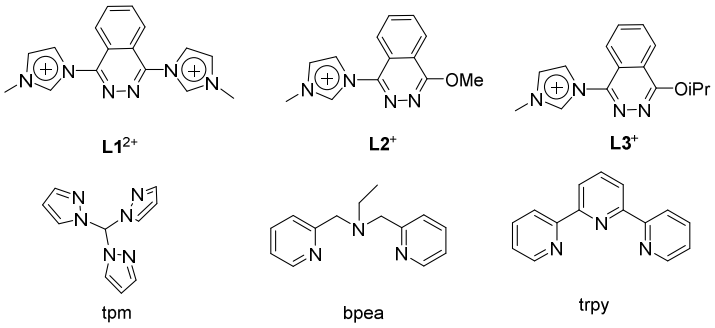

Chart 1. Drawing of the NHC (**L1**$^{2+}$) and N-donor (trpy, bpea and tpm) ligands proposed to be combined with Ru. R= Me o iPr.

Dalton Transactions

ARTICLE

Results and discussion

Synthesis of the ligand $L1^{2+}$. **L1**$(Cl)_2$ and **L1**$(PF_6)_2$ were obtained following a one-step nucleophilic attack of 1-methylimidazole to 1,4-dichlorophthalazine (dcp) in DMF (Scheme 1). The insolubility of **L1**$(Cl)_2$ in DMF allowed the easy isolation of the ligand by simple filtration and subsequent washing with diethyl ether (yield 75%). Subsequent treatment of **L1**$(Cl)_2$ with a NH_4PF_6 saturated solution in MeOH allowed the exchange of the chloride by the PF_6^- counterion (**L1**$(PF_6)_2$).

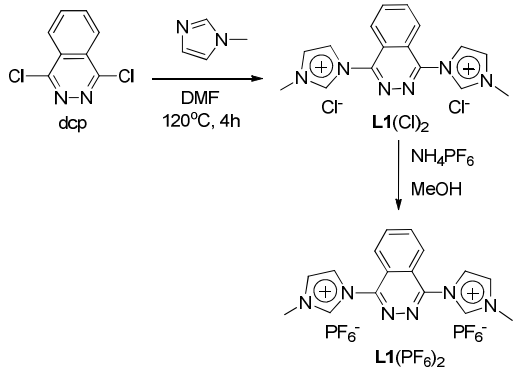

Scheme 1. Synthetic procedure for the synthesis of **L1**$(Cl)_2$ and **L1**$(PF_6)_2$.

Characterization of the ligand $L1^{2+}$. NMR spectroscopy for $L1^{2+}$ has been carried out both in acetone-d_6 (**L1**$(PF_6)_2$) and methanol-d_4 (**L1**$(Cl)_2$). Both 1D (^1H, ^{13}C) and 2D (COSY and HSQC) experiments were necessary to characterize the structure of the ligand in solution (Fig. 1 and Figure S1 in the Supporting Information). All resonances could be unambiguously assigned based on their integrals, multiplicity and the C_{2v} symmetry of the ligand in solution. For $L1^{2+}$, both H9 and H10 (or H9' and H10') display a doublet of doublets with a mirror effect, which is in agreement with the typical AA'BB' (9 9'10 10' in our case) pattern of this kind of systems,[10] as shown in the inset of Fig. 1. The singlet appearing at very low fields in acetone-d_6 (Fig. 1a) can be assigned to the imidazolic protons 6 and 6' in accordance with the high electron-withdrawing effect of the two heteroatoms present in α, as previously reported for similar ligands.[11] However, the integral of this resonance at 9.9 ppm sharply decreases (up to only 5% of the expected value) when the ^1H NMR spectrum of **L1**$(Cl)_2$ is recorded in methanol-d_4 (Fig. 1b), showing the fast exchange rate of these acidic protons with the protic solvent.

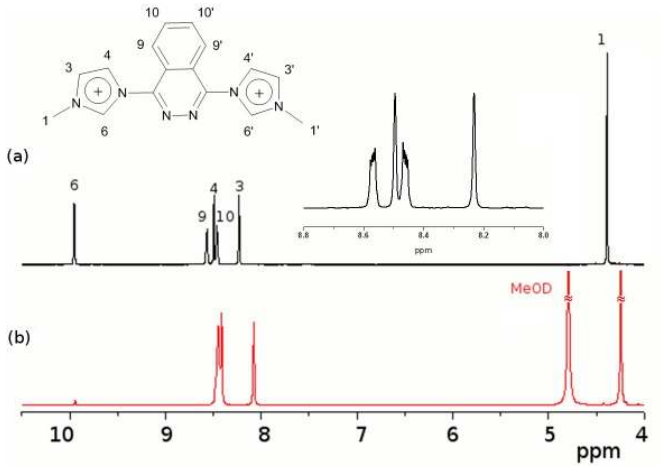

Figure 1. ^1H NMR spectrum of **L1**$(PF_6)_2$ in acetone-d_6 (a) and of **L1**$(Cl)_2$ in MeOD (b). Inset: zoom of the aromatic region of **L1**$(PF_6)_2$.

Suitable crystals for X-ray diffraction analysis were obtained by slow diffusion of diethyl ether into a solution of **L1**$(PF_6)_2$ in acetone (Fig. 2). It is worth mentioning that the steric congestion of both five membered rings with the central phthalazine moiety (specially protons H6'-H9' and H4-H9, at 2.4-2.5 Å) place the three scaffolds in different planes, with the left-side imidazole ring 42.5° below the phtalazine plane and the right-side imidazole ring 44.3° above (Fig. 2). The ORTEP plot for the cationic moiety of $L1^{2+}$ and the acquisition and crystallographic data for **L1**$(PF_6)_2$ can be found in Figure S2 and Table S1 in the Supporting Information, respectively.

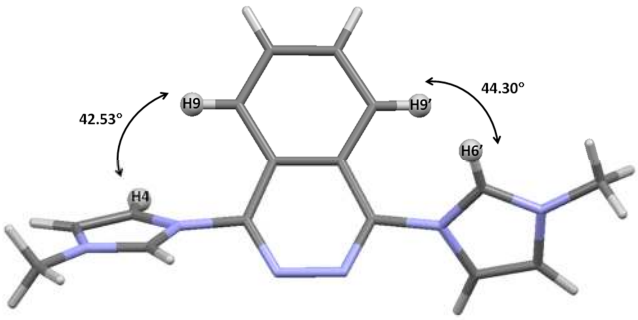

Figure 2. Mercury plot of the crystal structure of **L1**$^{2+}$. The hydrogen atoms at closer distances are shown as spheres, and the angles between the plane of two imidazoles and the phthalazine scaffold are included. Color code: nitrogen, blue; carbon, dark gray; hydrogen, light gray.

Reaction of L1^{2+} with [Ru(T)Cl$_3$] (T = trpy, tpm, bpea). Breakage of ligand L1^{2+} and synthesis of complexes 1a$^+$/2a^{2+}, 1b$^+$/2b^{2+}, 3$^+$/4^{2+} and 5$^+$/6^{2+}. Following previously reported synthetic strategies reported by our group[7b,10,12] 2 molar equivalents of [Ru^{III}(T)Cl$_3$] (T = trpy, tpm, bpea) were mixed with **L1**$^{2+}$, triethylamine (Et_3N) as reducing agent and LiCl to ensure the presence of a labile site in the generated complexes, and refluxed in MeOH for 16 h. After hot filtration, addition of a few drops of a saturated aqueous solution of NH_4PF_6 to the crude solution and partial solvent evaporation under vacuum, a brown precipitate appeared in all cases. However, despite bimetallic species with the general formula [Ru$_2^{II}$(T)$_2$(μ-Cl)(μ-**L1**)]$^{3+}$ or [Ru$_2^{II}$(T)$_2$(Cl)$_2$(μ-**L1**)]$^{2+}$ were expected, when the obtained compounds were subjected to ^{1}H NMR analysis, their resonances, integrals and coupling constants matched those of a mononuclear Ru complex. Furthermore, DOSY NMR experiments excluded the presence of mixed mono and dinuclear species. As an example, Fig. S3 in the Supporting Information shows the DOSY NMR spectrum for the mononuclear compound obtained after reflux of [Ru^{III}(trpy)Cl$_3$] with **L1**(Cl)$_2$ in MeOH.

Thus, although **L1**$^{2+}$ shows excellent stability in air and also dissolved in acetone or methanol at room temperature, it decomposes when refluxed overnight in the latter, therefore pointing to a replacement of one imidazole ring of **L1**$^{2+}$ by a methoxy group due to a nucleophilic attack of the solvent (Scheme S1 in the Supporting Information). This phenomenon has already been reported by other authors when using related tetradentate CNNC ligands in similar conditions.[13] Then, isopropanol, with increased steric hindrance compared to methanol, was also tested as solvent for the coordination of **L1**$^{2+}$ to Ru. However, the same process happened, with decomposition of the tetradentate ligand and formation of a mononuclear complex (Scheme 2). As a result, the new ligands PhthaPz-OMe (**L2**$^+$) and PhthaPz-OiPr (**L3**$^+$) have been obtained from **L1**$^{2+}$ (Scheme S1), which can only act as CN bidentate ligands towards Ru. The breakage of **L1**$^{2+}$ can also be explained from an electronic point of view, since when **L1**$^{2+}$ coordinates to a first electrophilic Ru(II) ion, there is a flow of electron-density from the ligand to the metal centre and, therefore, the nucleophilic attack of a MeOH or iPrOH solvent molecule becomes still more favourable.

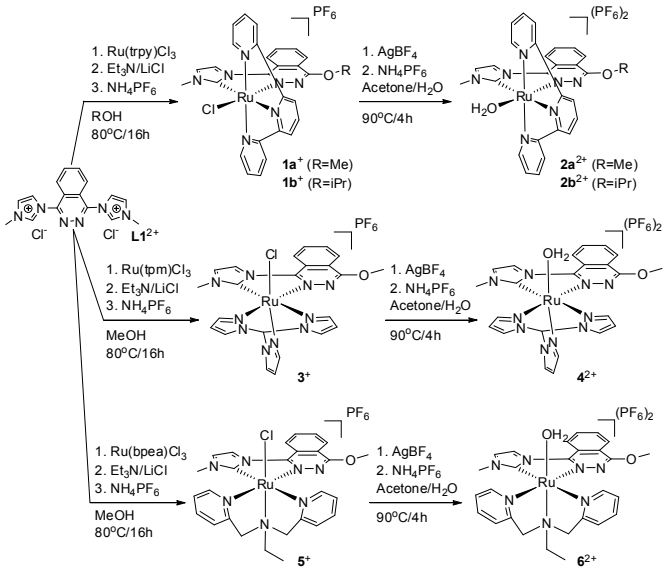

Scheme 2. Synthetic procedures used for the synthesis of **1a**$^+$/**2a**$^{2+}$, **1b**$^+$/**2b**$^{2+}$, **3**$^+$/**4**$^{2+}$ and **5**$^+$/**6**$^{2+}$. Note breakage of **L1**$^{2+}$ when refluxed in MeOH or iPrOH.

As a consequence, due to the breakage of **L1**$^{2+}$ in the conditions used, we adjusted the [Ru^{III}(T)Cl$_3$]:**L1**$^{2+}$ molar ratio to 1.5:1 in order to maximize the yield of formation of the Ru mononuclear species. Therefore, complexes **1a**$^+$ (*cis*-[Ru^{II}(PhthaPz-OMe)(trpy)Cl]PF$_6$), **1b**$^+$ (*cis*-[Ru^{II}(PhthaPz-OiPr)(trpy)Cl]PF$_6$), **3**$^+$ ([Ru^{II}(PhthaPz-OMe)(tpm)Cl]PF$_6$) and **5**$^+$ (*trans,fac*-[Ru^{II}(PhthaPz-OMe)(bpea)Cl]PF$_6$) were obtained in good yields. The subsequent synthesis of the corresponding aqua complexes involved the presence of $AgBF_4$ in acetone/H_2O, which promotes the decoordination of the chlorido ligand by formation of an AgCl precipitate and allows the coordination of a water molecule. After AgCl filtration, acetone was slowly evaporated under vacuum. The counter ion could be easily exchanged from BF_4^- to PF_6^- by adding excess NH_4PF_6(aq) into the aqueous solution, obtaining the whole set of Ru-aqua complexes [Ru(PhthaPz-OR)(T)(H$_2$O)](PF$_6$)$_2$ (R=Me, T=trpy, **2a**$^{2+}$; R=iPr, T=trpy, **2b**$^{2+}$; R=Me, T=tpm, **4**$^{2+}$; R=Me, T=bpea, **6**$^{2+}$) as red (or brown) precipitates (Scheme 2).

Structural characterization of complexes 1a$^+$/2a^{2+}, 1b$^+$/2b^{2+}, 3$^+$/4^{2+} and 5$^+$/6^{2+}. All mononuclear complexes have been characterised by spectroscopic (1D and 2D NMR) and spectrometric (ESI-MS) techniques and by elemental analysis (EA).

In the ^{1}H NMR spectrum of **1a**$^+$ (Fig. 3) the loss of the "ABBA" spin-spin coupling pattern perfectly agrees with the reduced symmetry of **L1**$^{2+}$ after nucleophilic decomposition. Furthermore, the two singlets integrating three protons each at 4.78 and 3.47 ppm can be assigned to the methyl group of the intact imidazole ring and the methyl group of the new methoxy substituent formed, respectively. Additional ^{13}C NMR and 2D-NMR spectra allowed full assignment of all resonances (see Figure S4 in the Supporting Information).

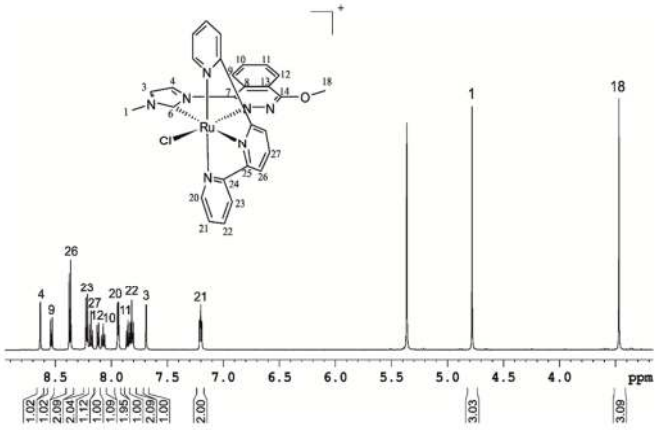

Figure 3. ^{1}H NMR spectrum of **1a**$^+$ in CD_2Cl_2 and its corresponding proton assignment.

As expected, a similar ^{1}H NMR spectrum to **1a**$^+$ was obtained for **1b**$^+$. However, now the singlet at 3.47 ppm assigned to the methoxy substituent in **1a**$^+$ is replaced by a doublet and a septuplet (at 1.09 and 4.54 ppm, integrating six and one protons, respectively) due to the presence of the isopropoxy substituent (Figure S5a in the Supporting Information). Furthermore, the integrity and purity of **1a**$^+$ and **1b**$^+$ was confirmed by EA and ESI-MS (Figure S8a-b in the Supporting Information).

The chlorido compounds **1a**$^+$ and **1b**$^+$ display C_s symmetry in solution, with the symmetry plane passing through the PhthaPz-OMe (**1a**$^+$) and PhthaPz-OiPr (**1b**$^+$) ligand, the Ru centre, the chlorido ligand and carbons C(27) (**1a**$^+$) or C(28) (**1b**$^+$) of the trpy ligand, interconverting the two sides of the molecule. Thus, with respect to the relative position of the chlorido ligand in relation to the Ru carbene bond, both the *cis* and *trans* isomer could be formed either for **1a**$^+$ or **1b**$^+$. However, only one isomer was obtained in the reaction crude for both **1a**$^+$ and **1b**$^+$, as determined by ^{1}H NMR (Fig. 3 and Figure S5a). 2D ROESY NMR spectra were then carried out to identify the *cis* or *trans* nature of the obtained compounds. As shown in Fig. 4 for the **1b**$^+$ case (see Figure S5e for the ROESY NMR spectra of the aromatic region of **1b**$^+$) strong interactions were observed between the isopropyl group and H24, H27 and H28 of the trpy ligand as well as between the methyl group of the imidazole ring and H21 of the trpy ligand, which clearly allow the identification of the *cis* disposition of the **1b**$^+$ complex. The same conclusion could be extracted from the ROESY NMR spectra of **1a**$^+$ (Figure S4e), and therefore the only obtained isomer is also *cis* in nature. Again, additional ^{13}C NMR and 2D-NMR spectra allowed full assignment of all resonances of **1b**$^+$ (Figure S5 in the Supporting Information).

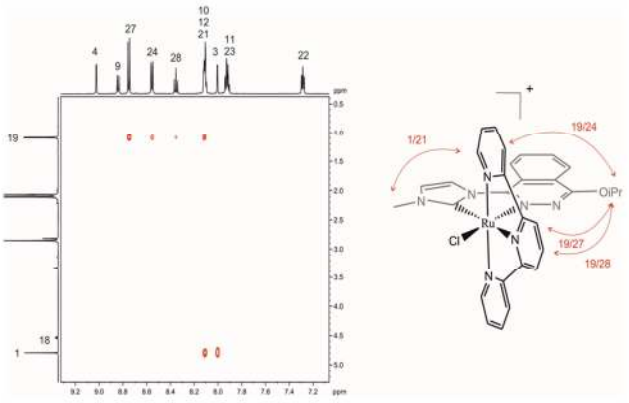

Figure 4. Selective 2D ROESY NMR spectrum of **1b**$^+$ in acetone-d_6 and schematic drawing of the observed interactions.

With regards to **3**$^+$, due to the C_3 symmetry of the tpm ligand, which coordinates in a facial manner, no isomeric mixtures are expected. This has been corroborated by its ^{1}H NMR spectrum (Figure S6a). The C_1 symmetry of the complex converts the whole set of protons in different resonances and a complex spectrum is obtained. The assignment of each resonance to a single proton and carbon was carried out by 2D NMR experiments (HSQC, HMBC, ROESY and TOSCY), while the integrity and purity of **3**$^+$ was confirmed by EA and ESI-MS (see Figures S6 and Figure S8c, respectively, in the Supporting Information).

Concerning **5**$^+$, due to the flexibility of the tridentate bpea ligand, able to potentially coordinate the Ru metal ion either facially or meridionally,[14] seven stereoisomers could be potentially formed when combining bpea with the non-symmetric bidentate CN ligand PhthaPz-OMe (Fig. 5).[15] The notation *fac* and *mer* refers to the facial or meridional disposition of the bpea ligand, respectively, whereas *up* and *down* indicates the relative orientation of the ethyl group of bpea with regards to the chlorido ligand upon coordination. In the *fac* complexes, the *cis*/*trans* notation refers to the position of the chlorido ligand with respect to the aliphatic N atom of the bpea ligand, while in the *mer* cases the *cis*/*trans* notation refers to the position of the chlorido ligand with respect to the carbene atom of the PhtaPz ligand. Both steric and electronic interactions between the ligands coordinated to the Ru metal ion play a key role in the degree of the isomeric mixture synthetically obtainable. However, in the synthesis of **5**$^+$, only the *trans*,*fac* isomer is formed (see below). Hydrogen bonding interactions between the protons in α to the pyridylic nitrogens of bpea and the chlorido ligand dramatically stabilize the *trans,fac* conformation, lowering the energy of the system. This strong stabilitzation for the *trans,fac* isomer has already been reported and thoroughly studied by means of theoretical DFT calculations for similar Ru-based systems,[16] and the predominance of these hydrogen-bonding interactions over other factors for stabilizing and selectively obtaining the *trans,fac* isomer in a series of related complexes has been already established by several research groups.[17] Furthermore, it has also been reported the preference of bpea for the facial coordination upon heating (thermodynamic conditions).[14]

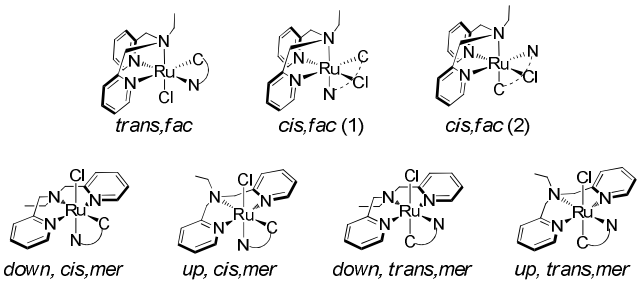

Figure 5. Possible diastereomers for $\mathbf{5}^{+}$. The PhthaPz-OMe ligand is represented as a CN connector for the sake of clarity. SENSE ESPAIS

Effectively, the *trans,fac* nature of the $\mathbf{5}^{+}$ complex was confirmed by selective NOESY NMR experiments, whose key interactions unambiguously revealed its stereoisomeric nature (Figure S7e-f in the Supporting Information). Thus, interactions between H1 and H20-H21 and between H18 and H34 are observed, confirming its *trans,fac* configuration. In consequence, analogously to what happened with $\mathbf{3}^{+}$, no symmetry is observed in its ^{1}H NMR spectrum (Fig. 6)**.** Finally, the assignment of each resonance to a single proton and carbon was carried out by 2D NMR experiments (HSQC, ROESY), while the integrity and purity of $\mathbf{5}^{+}$ was confirmed by EA and ESI-MS (see Figures S7 and Figure S8d, respectively, in the Supporting Information).

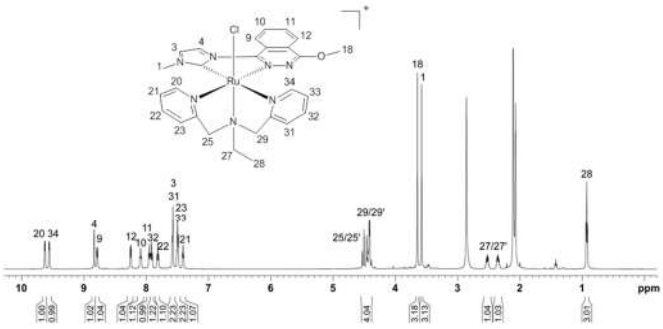

Figure 6. ^{1}H NMR spectrum of $\mathbf{5}^{+}$ in acetone-d_6 and its corresponding proton assignment.

Suitable crystals for X-ray diffraction analysis of $\mathbf{5}^{+}$ were obtained by slow diffusion of diethyl ether into a solution of the complex in methanol (Fig. 7), and a selection of the more relevant bond distances and angles is reported in Table S2. An ORTEP plot for the cationic moiety of this complex as well as that corresponding to its unit cell can be found in Figure S9 of the Supporting Information. Thus, $\mathbf{5}^{+}$ crystallizes in a small unit cell containing two PF_6^- anions located in its centre and two independent complex molecules, each one located on each side of the PF_6^- anions. Additionally, a complete description of the acquisition and crystallographic data can be found in Table S3 of the Supporting Information.

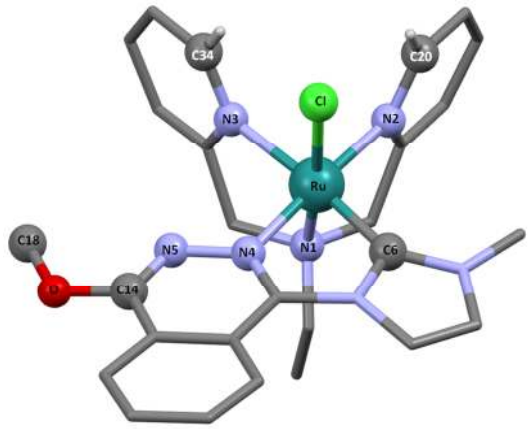

Figure 7. Mercury plot of the crystal structure of the cationic part of $\mathbf{5}^{+}$. Hydrogen atoms have been removed for the sake of clarity except those involved in hydrogen-bonding interactions with the Cl^- ligand. Color code: nitrogen, blue; oxygen; red; chlorine, green; carbon, dark gray; hydrogen, light gray. Atoms appearing in Table S2 or throughout the text are depicted as spheres that have been labelled accordingly.

The Ru(II) ion adopts a distorted octahedral geometry with bond distances and angles that resemble those of analogous complexes reported in earlier literature.[15b,18] The Ru carbene bond distance (1.962 Å) is shorter than the Ru-N bonds, which are comprised between 2.0 and 2.1 Å. The N1-Ru-Cl (171.63°), N2-Ru-Cl (94.92°) and N3-Ru-Cl (90.90°) bond angles clearly confirm the facial coordination of bpea to Ru. Plus, the Ru-Cl bond appears *trans* to the aliphatic N atom of bpea, confirming again the *trans*,*fac* nature of $\mathbf{5}^{+}$. Furthermore, the imidazole and the phthalazine rings do not lay exactly on the same plane. Instead, there is a torsion angle of 16°. However, this angle is obviously shorter with regards to the one observed for the free ligand, which is around 43° (Fig. 2). The methoxy group is nearly on the same plane of the phthalazine skeleton, since the observed torsion angle C18-O-C14-N5 is only 1.9°. Finally, the N1-Ru-N3 and N1-Ru-N2 angles are, respectively, 81.15° and 81.68°, away from the 90° for an ideal octahedral geometry, due to the formation of two five-membered rings when bpea coordinates to the central Ru ion. In addition, clear hydrogen-bonding interactions are observed between the pyridyl protons of bpea on C20 and C34 and the chlorido ligand (2.7 Å). This electronic interaction is responsible for the strong stabilization of the *trans,fac* configuration of $\mathbf{5}^{+}$, as stated before.[16,17]

Replacement of the chlorido ligand by a water molecule in this family of complexes induces significant chemical shift displacements. This is exemplified by the $\mathbf{1a}^{+}/\mathbf{2a}^{2+}$ ^{1}H NMR comparison shown in Fig. S10, where mainly protons close to these monodentate ligands such as H22, H26 and H27 are affected. Similar displacements of the chemical shifts were obviously observed for the very similar $\mathbf{1b}^{+}/\mathbf{2b}^{2+}$ couple, and both complexes maintain their *cis* conformation after the coordination of the aqua ligand (see Figures S11 and S12, respectively, for a full NMR assignment of all proton and carbon resonances of $\mathbf{2a}^{2+}$ and $\mathbf{2b}^{2+}$).

Complexes $\mathbf{4}^{2+}$ and $\mathbf{6}^{2+}$ also maintain their original conformation in solution after chloride displacement, as can be deduced from the NMR spectra shown in Figures S13 and S14 in the Supporting Information, respectively. Furthermore, the integrity and purity of

all four aqua complexes was confirmed by EA and ESI-MS (Figure S15 in the Supporting Information).

Electrochemical and spectrophotometric characterization of complexes $\mathbf{1a}^{+}/\mathbf{2a}^{2+}$, $\mathbf{1b}^{+}/\mathbf{2b}^{2+}$, $\mathbf{3}^{+}/\mathbf{4}^{2+}$ and $\mathbf{5}^{+}/\mathbf{6}^{2+}$. CV and DPV techniques have been used to determine the electrochemical properties of all complexes. The CVs in dichloromethane of complexes $\mathbf{1a}^{+}$, $\mathbf{1b}^{+}$, $\mathbf{3}^{+}$ and $\mathbf{5}^{+}$ are depicted in Figure S16 in the Supporting Information. All chlorido complexes exhibit a single reversible wave corresponding to the Ru^{III}/Ru^{II} process. The redox potentials vs SCE are very close for $\mathbf{1a}^{+}$ (0.79 V) and $\mathbf{1b}^{+}$ (0.78 V) given the high structural and chemical similarity of Ru in both meridional complexes, while a clear downshift of $E_{1/2}$ is observed for the facial derivatives $\mathbf{3}^{+}$ (0.71 V) and $\mathbf{5}^{+}$ (0.68 V). This is in agreement with the higher σ-donating and lower π-acceptor capacity of both the pyrazolyl rings ($\mathbf{3}^{+}$) and the aliphatic N ($\mathbf{5}^{+}$) with regards to the pyridyl units of the trpy scaffold. The observed decrease in the redox potentials lies within a 70-110 mV range and is in agreement with previous results obtained for analogous Ru carbene complexes containing trpy or bpea.[15b]

The redox behaviour of the four Ru-OH_2 complexes has been extensively investigated in aqueous media and their redox potentials and pKa values are summarized in Table 1, together with those of related aqua complexes containing the bpy ligand instead of the carbene bidentate scaffold for the sake of comparison.

Table 1. Redox potentials (V) vs SCE and pKa values of complexes $\mathbf{2a}^{2+}$ to $\mathbf{6}^{2+}$ and related aqua complexes where the carbene bidentate scaffold has been replaced by bpy.

Entry		$E_{1/2}^{III/II}$		$E_{1/2}^{IV/III}$	$E_{1/2}^{III/II}$	$\Delta E_{1/2}$ [c]	$E_{1/2}^{V/IV}$			Ref.
		pH 1 [a]	iv/ii		pH 7 [b]			pKa_1	pKa_2	
1	$\mathbf{2a}^{2+}$	0.74	0.50	0.52	0.49	0.03	1.29	3.0	11.5	d
2	$\mathbf{2b}^{2+}$	0.73	0.49	0.51	0.48	0.03	---	2.8	11.0	d
3	$\mathbf{4}^{2+}$	0.62	--	---	0.35	---	1.33	1.8	11.2	d
4	$\mathbf{6}^{2+}$	0.61	0.42	0.52	0.32	0.20	1.28	1.2	11.7	d
5	$[Ru(trpy)(bpy)(OH_2)]^{2+}$	0.81	0.55	0.62	0.49	0.13	---	1.7	9.7	19
6	$[Ru(tpm)(bpy)(OH_2)]^{2+}$	0.70	0.55	0.71	0.40	0.31	---	1.9	10.8	20
7	$[Ru(bpea)(bpy)(OH_2)]^{2+}$	0.70	0.40	0.46	0.34	0.12	---	1.2	11.1	21

[a] 0.1 M triflic acid. [b] phosphate buffer solution (μ = 0.1 M). [c] $\Delta E_{1/2} = (E_{1/2}^{IV/III} - E_{1/2}^{III/II})$. [d] This work.

At pH 1, a single reversible wave corresponding to the Ru^{III}-OH_2/Ru^{II}-OH_2 process is observed for all aqua complexes (black lines in Figures S17, S19, S21 and S22 in the Supporting Information), in which again a cathodic shift of $E_{1/2}$ (110-130 mV) takes place when introducing the facial ligands (entries 3-4 vs. entries 1-2, Table 1), following the same trend observed for the Ru-aqua complexes bearing bpy instead of the bidentate carbene ligand (entries 5-7, Table 1).

At neutral pH, two very close redox processes separated by only 30 mV can be observed for $\mathbf{2a}^{2+}$ and $\mathbf{2b}^{2+}$, corresponding to the Ru^{IV}-O/Ru^{III}-OH and Ru^{III}-OH/Ru^{II}-OH_2 processes (red lines in Figures S17 and S19), thus making the stability region of the Ru(III) species very small ($\Delta E_{1/2}$ = 30 mV, Table 1). The decrease in the stability region of Ru(III) when introducing carbene ligands in Ru polylyridilic complexes has already been described,[8,15b] which can be confirmed in our case if comparing with the $\Delta E_{1/2}$ value for $[Ru(trpy)(bpy)(OH_2)]^{2+}$ (130 mV, Table 1). This tendency, however, can be reversed when replacing the trpy ligand in $\mathbf{2a}^{2+}$ and $\mathbf{2b}^{2+}$ by the facial aliphatic ligand bpea (Figure S22), since the higher σ-donating and lower π-acceptor capacity of bpea provoke a stabilization of the Ru(III) state[21] (lowering the $E_{1/2}^{III/II}$ potential by 160-170 mV while keeping $E_{1/2}^{IV/III}$ unaltered, entries 1-2 and 4, Table 1). Consequently, $\Delta E_{1/2}$ is 200 mV for $\mathbf{6}^{2+}$. Unfortunately, for the tpm derivative $\mathbf{4}^{2+}$ the Ru^{IV}-O/Ru^{III}-OH process could not be detected (Figure S21). The absence of the Ru(IV/III) redox couple in CV experiments is quite common for aqua complexes and is due to slow heterogeneous electron-transfer kinetics from the solution to the electrode surface.[22] Finally, the effect of the higher σ-donating character of the carbene ligand compared to bpy is evidenced when comparing the $E_{1/2}^{III/II}$ values of $\mathbf{4}^{2+}$ and $[Ru(tpm)(bpy)(OH_2)]^{2+}$ (cathodic shift of 50 mV, entries 3 and 6, Table 1).

The simultaneous removal of protons and electrons (PCET processes) taking place for the four aqua-complexes can be observed in their Pourbaix diagrams (Fig. 8 and Figure S20), which have allows measuring their pKa_1 (Ru^{III}-OH_2) and pKa_2 (Ru^{II}-OH_2) values. Thus, the aqua groups of $\mathbf{6}^{2+}$ (bpea) and $\mathbf{4}^{2+}$ (tpm) for the Ru(III) state are more acidic than those corresponding to their meridional (trpy) counterparts (pka_1 values of 1.2 and 1.8 vs 3.0-2.8, Table 1), while no significant differences are observed among the pKa_2 values. Finally, higher acidities are observed for their non-carbene analogues (lower pka_1 and specially pka_2 values, entries 5-7, Table 1), given the lower σ-donating character of bpy compared to the carbene bidentate ligand.

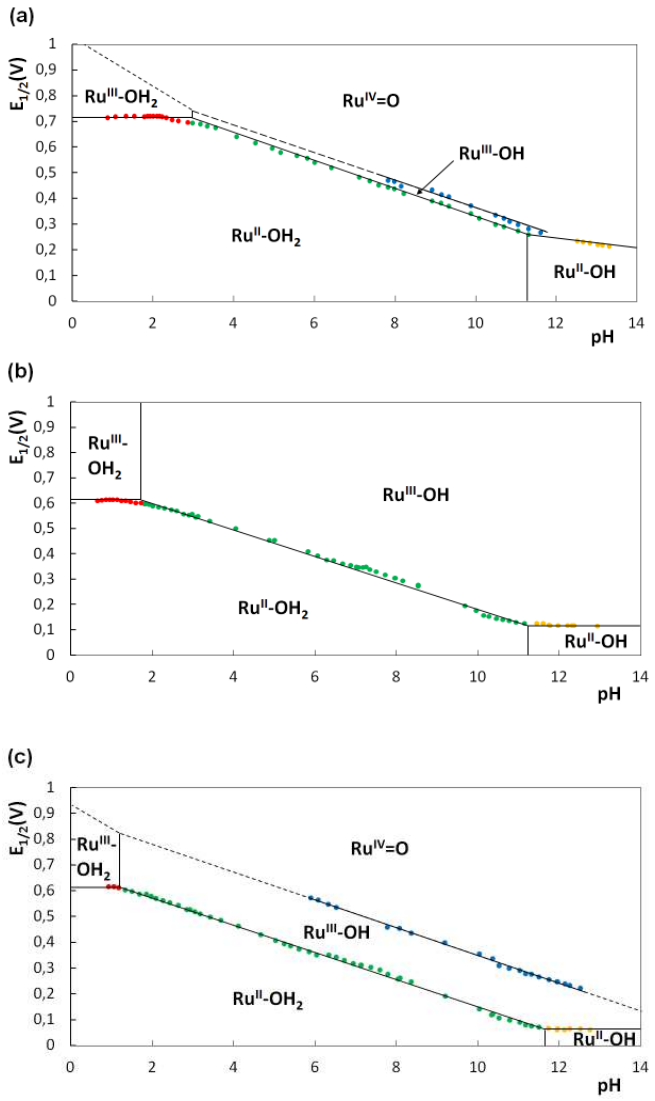

Figure 8. Plot of $E_{1/2}$ vs pH (Pourbaix diagram) for complexes $\mathbf{2a}^{2+}$ (a), $\mathbf{4}^{2+}$ (b) and $\mathbf{6}^{2+}$ (c). The pH/potential regions of stability for the various oxidation states and their dominant proton compositions are indicated by using abbreviations such as Ru^{II}-OH_2, for example, for $[Ru^{II}(L2)(OH_2)(T)]^{2+}$ (T = trpy, tpm, bpea). The vertical lines in the various E/pH regions show the pKa values.

Also, in order to confirm the correspondence of all observed redox waves to mono-electronic electrochemical processes, bulk electrolysis experiments were carried out at pH 4.9 for the aqua complexes (Figure S18 in the Supporting Information). Thus, for $\mathbf{2a}^{2+}$ at 0.75 V vs SCE (just after the predicted potential of the second redox wave) a value of 2.06 electrons per complex molecule was obtained (Figure S18a), while for $\mathbf{4}^{2+}$ at 0.6 V (after the potential of the unique redox wave observed) a value of 0.97 electrons per molecule was obtained (Figure S18b). Finally, the stability of the Ru^{III}-OH species and the stepwise mono-electronic nature of both $Ru^{III/II}$ and $Ru^{IV/III}$ processes have been confirmed for $\mathbf{6}^{2+}$, since after applying a potential of 0.57 V vs SCE (just after the expected potential of the first redox process), a value of 0.91 electrons per molecule was obtained (Figure S18c), while when the potential was set at 0.75 V, 1.87 electrons were transferred per molecule (Figure S18d). In summary, from an electronic point of view all aqua complexes favour mono-electronic transfers between Ru(II), Ru(III) and Ru(IV). AQUI PODRIA SER XULO CALCULAR EL POTENCIAL iv/ii I ESPECULAR UNA MICA SOBRE LA TENDENCIA DEL iv D'ANAR DIRECTEAMENT A ii O A iii. However for $\mathbf{2a}^{+}$ and $\mathbf{2b}^{+}$ their tendency for IV/II reaction is very similar to the one electron transfer processes whereas in all the other cases the 1 electron transfer process is clearly favoured.

The UV-vis spectra of the eight complexes described in this work have been recorded in methanol and are displayed in Figure S23 in the Supporting Information. Two regions can be observed in all cases: one region between 260 nm and 350 nm (or 325 nm for $\mathbf{5}^{+}$/$\mathbf{6}^{2+}$) with very intense bands due to intra ligand π-π* transitions, and a second one between 350 nm (or 325 nm for $\mathbf{5}^{+}$/$\mathbf{6}^{2+}$) and 550 nm, where typical broad unsymmetrical metal-to-ligand charge transfer (MLCT) bands appear, which could be tentatively assigned to Ru(*d*π)-N ligand(π*) transitions.[19,21] Also, the electronic nature of the monodentate ligand influences to some extent the energies of the transitions involving Ru *d* orbitals. Thus, the MLCT bands for the Ru-aqua complexes are blue-shifted with regards to those of their Ru-Cl counterparts due to the relative stabilization of the Ru(*d*π) levels provoked by the non-π-donor character of the aqua ligand.

Electrochemical and chemical water oxidation by complexes $\mathbf{2a}^{2+}$, $\mathbf{2b}^{2+}$, $\mathbf{4}^{2+}$ and $\mathbf{6}^{2+}$. The capacity of the aqua complexes to oxidize water into dioxygen was initially tested electrochemically. For this purpose, the CVs of $\mathbf{2a}^{2+}$, $\mathbf{4}^{2+}$ and $\mathbf{6}^{2+}$ were recorded in aqueous solution at pH 1.0 until redox potentials were high enough to reach the oxidation states potentially able to oxidize water. Accordingly, a large electrocatalytic wave above 1.4 V vs SCE corresponding to the oxidation of water to dioxygen was observed in all cases (see below).

In order to obtain kinetic information about the catalytic process, a "foot of the wave analysis" (FOWA)[23] was carried out to calculate the apparent rate constant k_{obs}. For that purpose we followed the equations adapted for water oxidation recently reported.[24] Thus, under catalytic conditions, equation 1 is operative:

$$\frac{i}{i_p^0} = \frac{8.96\sqrt{\frac{RT}{Fv}k_{obs}}}{1+\exp\left[\frac{F}{RT}\left(E_{PQ}^0 - E\right)\right]} \quad (1)$$

where E^0_{PQ} is the standard potential for the catalysis-initiating redox couple (which corresponds to the pH independent $Ru^{V}O/Ru^{IV}O$ wave, observed at 1.29 V for $\mathbf{2a}^{2+}$, at 1.33 V for $\mathbf{4}^{2+}$ and at 1.28 V for $\mathbf{6}^{2+}$ according to the DPVs shown in Figure S26 in the Supporting Information and shown in Table 1), *i* is the CV current intensity in the presence of substrate, i^0_p is the peak current intensity of a one-electron redox process of the catalyst (we approximate this current to the current associated with the Ru^{III}/Ru^{II} couple), *F* is the Faradaic constant, ν is the scan rate and R is 8.314 $J{\cdot}mol^{-1}{\cdot}K^{-1}$, thus allowing the extraction of k_{obs}. As an example, Fig. 9 shows the CV of a 0.69 mM solution of $\mathbf{4}^{2+}$ at pH 1.0 (Fig. 9a) and the plot of i/i^0_p vs $1/\{1+\exp[(F/RT)(E^0_{PQ}-E)]\}$ (Fig. 9b) as well as the dependence of k_{obs} on catalyst concentration (Fig. 9b, inset). Identical studies have

been performed for **2a**$^{2+}$ and **6**$^{2+}$, which can be found in Figure S25 in the Supporting Information.

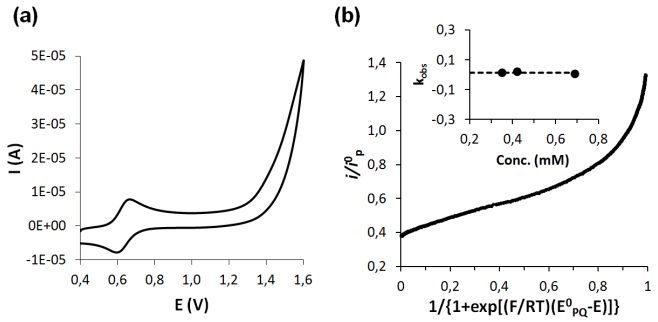

Figure 9. Background corrected CV of a 0.68 mM solution of **4**$^{2+}$ in aqueous triflic acid 0.1 M (pH 1.0) at 100 mV/s scan rate (a), and "foot of the wave analysis" of **4**$^{2+}$ by plotting i/i^0_p vs $1/\{1+\exp[(F/RT)(E^0_{PQ}-E)]\}$ (b). Inset: plot of the different k_{obs} values extracted from the "foot of the wave analysis" at each concentration (the dotted line represents the trend of the k_{obs} values).

In all cases, the largest slope at the very beginning of the catalytic process (which translates to the foot of the wave in the original CVs) gives the value of k_{obs}, which is independent of catalyst concentration, ~~probably~~ indicating the existence of a water nucleophilic attack (WNA) mechanism.[25] Moreover, under the used electrocatalytic scheme, k_{obs} is equivalent to the maximum turnover frequency (TOF_{max}) that a catalyst molecule can operate the water oxidation reaction when the applied potential tends to infinite.[23] At pH 1.0, the obtained k_{obs} values (expressed in s^{-1}) follow the trend **2a**$^{2+}$ (0.570) > **6**$^{2+}$ (0.051) > **4**$^{2+}$ (0.015).

Finally, the relationship between the turnover frequency TOF and the overpotential (η), defined as the difference between the applied potential *E* and the thermodynamic potential of the catalysed reaction E^0_{AC}, in this case water oxidation, is governed by equation 2, whose logarithms for all three aqua compounds at pH 1.0 are plotted in Figure 10 (catalytic Taffel plots).

$$TOF = \frac{k_{obs}}{1+\exp\left[\frac{F}{RT}(E^0_{PQ}-E^0_{AC}-\eta)\right]} \quad (2)$$

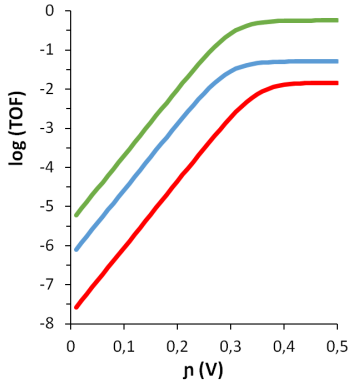

Figure 10. Catalytic Taffel plots for **2a**$^{2+}$ (green), **4**$^{2+}$ (red) and **6**$^{2+}$ (blue) at pH 1.0.

Fig. 10 shows how the higher value of E^0_{PQ} for **4**$^{2+}$ (1.33 V, Table 1) translates in lower turnover frequencies when η is low (red line before reaching the plateau, when η makes TOF reach its maximum and equals k_{obs}). Also, it is made evident the higher performance of **2a**$^{2+}$ (green line), in concordance with the higher k_{obs} values deduced by the "foot of the wave analysis". However, it should be noted that the kinetic parameters for catalytic reactions derived from electrochemical measurements depend on various details of the experimental procedures, and therefore values from different studies should be compared carefully.[26]

The four aqua complexes were also tested as chemically triggered water oxidation catalysts in the presence of Ce(IV) as sacrificial oxidant. The total gas evolved was manometrically measured (Figure S27 in the Supporting Information) and its composition in terms of O_2:CO_2 ratio was analyzed by means of on-line Mass Spectrometry (Figure S28). In the presence of 100 equivalents of Ce(IV) at pH 1, **4**$^{2+}$ generated more gas (≈ 15 mBar) after 30 min of reaction than the other three complexes (Figure S28). In general, and only considering the amount of generated gas, facial complexes are superior to their meridional counterparts. However, when the composition of the generated gases is analyzed by on-line MS (Figure S28), **4**$^{2+}$ has the lowest O_2:CO_2 ratio (1:5.5), followed by **6**$^{2+}$, with a 1:1.4 ratio, since the O_2:CO_2 ratio was much higher for **2a**$^{2+}$ and **2b**$^{2+}$ (1:0.6). Therefore, despite still poor, the stability of the meridional trpy-based complexes **2a**$^{2+}$/**2b**$^{2+}$ is clearly higher than that of their facial (tpm or bpea) counterparts **4**$^{2+}$/**6**$^{2+}$, that easily get oxidized in the harsh reaction conditions of chemical water oxidation by Ce(IV) at pH = 1.0. This is clearly reflected in Figure S29, where the profile of O_2 evolution of the four aqua complexes has been compared. Therefore, if taking into account the volume of the vial (16.04 mL) and the amount of catalyst used (2.0 μmol), the turnover numbers (TN) at 298K for **2b**$^{2+}$ and **2a**$^{2+}$ (2.39 and 2.17, respectively) are higher than those of **6**$^{2+}$ (1.63) and **4**$^{2+}$ (0.75). Moreover, this behaviour is consistent with the results obtained during the electrochemically triggered water oxidation at pH 1.0, with the highest TOF value corresponding to the trpy derivatives (**2a**$^{2+}$/**2b**$^{2+}$) and the lowest one to the tpm complex (**4**$^{2+}$).

Catalyst-catalyst intermolecular oxidative degradation involving Ru^{IV}=O species[27] or the direct degradation of the complexes by the highly oxidant Ce(IV) species are considered as the potential origin of the evolved CO_2. In our system, the only relevant differences between the four evaluated complexes are the tridentate ligands employed. Therefore, tpm and bpea (both containing aliphatic carbon atoms prone to be easily oxidized in the harsh catalytic conditions employed) quickly decompose generating large amounts of CO_2 that arise from ligand oxidation. Given that a great number of robust water oxidation catalysts containing the trpy ligand have been reported,[Error! Bookmark not defined.,28] the observed evolution of CO_2 from **2a**$^{2+}$/**2b**$^{2+}$ clearly reflects a relative weakness of the PhthaPz-OR family of ligands under oxidative conditions.

Electrochemical and chemical alkene epoxidation by complexes 2a^{2+}, 2b^{2+}, 4^{2+} and 6^{2+}. The capacity of the aqua complexes **2a**$^{2+}$, **4**$^{2+}$ and **6**$^{2+}$ to electrocatalytically epoxide *cis*-β-methylstyrene has been investigated by CV. All experiments were performed in DCM under well-controlled concentrations of catalyst and substrate, whose concentration was steadily increased. In all cases, the presence of

the alkene provoked significant electrocatalytic currents due to its oxidation from 1.2 V vs Hg/Hg_2SO_4 onwards (see Figures S30, S33 and S36 in the Supporting Information).

The rate constant value k for the electrocatalytic epoxidation reaction can be estimated from the plot of I_{cat} vs the square root of substrate concentration according to equation 3:[29]

$$I_{cat} = nFA[cat]D^{1/2}k^{1/2}[subs]^{1/2} \quad (3)$$

where I_{cat} is the current intensity in the presence of *cis*-β-methylstyrene, n is the number of electrons involved in the catalysis, F is the Faraday constant, A is the surface area of the working electrode in cm^2 (0.07 cm^2 in our case), [cat] is the concentration of catalyst in mM, D is the diffusion coefficient of the catalyst in cm^2/s and [subs] is the concentration of *cis*-β-methylstyrene in mM.

The plot of I_{cat} vs $[subs]^{1/2}$ shows a linear trend with the increasing concentration of substrate and, under kinetic control conditions, the slope is proportional to $k^{1/2}$ (see Figures S31, S34 and S37 in the Supporting Information). In order to estimate the value of the rate constant, the diffusion coefficient D was calculated from the peak current prior the addition of the substrate according to equation 4:[29]

$$I_p = 2.69\cdot10^5 n^{3/2} A D^{1/2} [cat] \nu^{1/2} \quad (4)$$

where I_p is the current intensity at 1.6 V vs Hg/Hg_2SO_4, n is the number of electrons involved in the electrochemical process, A is the surface area of the working electrode in cm^2, D is the diffusion coefficient of the catalyst in cm^2/s, [cat] is the concentration of catalyst in mM and ν is the scan rate in V/s. If a linear relationship for I_p vs $\nu^{1/2}$ is obtained, the slope is proportional to $AD^{1/2}$. As shown in Figures S32, S35 and S38 in the Supporting Information, the plot of I_p vs $\nu^{1/2}$ presents a good linear trend for the 20 - 200 mV/s range, and consequently the D values have been obtained, varying from $1.1\cdot10^{-4}$ ($\mathbf{6}^{2+}$) to $2.0\cdot10^{-4}$ cm^2/s ($\mathbf{2a}^{2+}$ and $\mathbf{4}^{2+}$).

From the combination of equations 3 and 4 the rate constants (k) of the three tested aqua complexes were calculated. Contrarily to what was observed when employing this set of catalysts in the chemical oxidation of water at pH 1.0 (where the decomposition of both the facial complexes $\mathbf{4}^{2+}$ and $\mathbf{6}^{2+}$ was extremely fast), now $\mathbf{6}^{2+}$ is by far the most efficient electro-catalyst for the epoxidation of *cis*-β-methylstyrene in DCM (k = 961 $M^{-1}\cdot cm^{-1}$ for $\mathbf{6}^{2+}$ compared to 576 and 441 $M^{-1}\cdot cm^{-1}$ for $\mathbf{2a}^{2+}$ and $\mathbf{4}^{2+}$, respectively). The different oxidation states involved in Ru mononuclear complexes (Ru(IV) for the epoxidation of a double bond and Ru(V) for the oxidation of water) may be the reason for the different relative efficiency in these two oxidative transformations of the set of aqua complexes here studied.

Complexes $\mathbf{2a}^{2+}$, $\mathbf{4}^{2+}$ and $\mathbf{6}^{2+}$ have also been tested with regards to their ability to chemically oxidize alkenes. The catalytic reactions have been carried out using a catalyst:substrate:oxidant:water ratio of 1:1000:2000:2000 after a 120 min mixing period of the catalysts in the absence of substrate (see Experimental Section for further details), during which the excess of water ensures the generation of the oxidant PhIO species from $PhI(OAc)_2$.[12,30] This mixing period before substrate addition is crucial in order to improve the rate of the catalytic reaction. Scheme S2 summarizes the set of reactions that take place during the catalytic epoxidation of alkenes for the proposed systems. All products of each catalytic experiment have been identified by GC-MS, and all gathered results are shown in Table 2. For instance, the system: $\mathbf{2a}^{2+}$ 1.7 mM, *cis*-β-methylstyrene 1.7 M, $PhI(OAc)_2$ 3.4 M, H_2O 3.4 M in DCE (entry 2) gives 1.42 M of *cis*-β-methylstyrene oxide in 525 minutes, which represents a TN value of 840 and a TOF value of 1.6 min^{-1}, and since the conversion of the initial substrate is complete the selectivity in the epoxide formation is 84%.

Table 2. Catalytic performance of $\mathbf{2a}^{2+}$ to $\mathbf{6}^{2+}$ in the epoxidation of *cis*- and *trans*-alkenes using PhIO as oxidant in DCE.[a]

Cat.	Entry	Alkene	Conv. (%)[b]	Selec. (%)[c]	TN/TOF[d]
$\mathbf{2a}^{2+}$	1	styrene	42	46	194/0.8
	2	*cis*-β-methylstyrene	>99	84[e]	840/1.6
	3	*trans*-stilbene[f]	>99	68	680/1.3
	4	cyclooctene	>99	93	930/1.9
$\mathbf{2b}^{2+}$	5	styrene	29	66	191/1.1
	6	*cis*-β-methylstyrene	>99	82[e]	816/1.3
	7	*trans*-stilbene[f]	>99	60	596/1.1
	8	cyclooctene	99	96	946/2.2
$\mathbf{4}^{2+}$	9	styrene	23	26	60/0.5
	10	*cis*-β-methylstyrene	97	56[e]	545/0.4
	11	*trans*-stilbene[f]	90	16	148/0.3
	12	cyclooctene	>99	76	756/0.3
$\mathbf{6}^{2+}$	13	styrene	21	13	27/0.1
	14	*cis*-β-methylstyrene	99	69[e]	687/0.7
	15	*trans*-stilbene[f]	91	15	136/0.2
	16	cyclooctene	>99	94	940/0.4

[a] Catalyst:substrate:oxidant:water ratio of 1:1000:2000:2000. See Experimental Section for further details. [b] Substrate conversion = {[substrate]initial - [substrate]final}/[substrate]initial·100. [c] Epoxide selectivity = [epoxide]final/{[substrate]initial-[substrate]final}·100. [d] TN is the turnover number with regard to the total epoxide obtained. TOF is the turnover frequency expressed in epoxide cycles per minute (TN/min). [e] *cis* epoxide. [f] DCE volume is 5 mL.

Similar figures are obtained for both trpy-based aqua-complexes ($\mathbf{2a}^{2+}$/$\mathbf{2b}^{2+}$) on the one hand and for both facial derivatives ($\mathbf{4}^{2+}$/$\mathbf{6}^{2+}$) on the other. Also, when comparing both sets of catalyst pairs, a clearly higher epoxidation capacity (higher conversion and selectivity) is observed for $\mathbf{2a}^{2+}$/$\mathbf{2b}^{2+}$ compared to $\mathbf{4}^{2+}$/$\mathbf{6}^{2+}$. For example, for styrene $\mathbf{2a}^{2+}$ yields a 42% conversion (entry 1), while $\mathbf{4}^{2+}$ and $\mathbf{6}^{2+}$ only reach 23 and 21% conversion, respectively (entries 9 and 13), and selectivity for $\mathbf{2b}^{2+}$ is 66% (entry 5) while it is only 26% and 13% for $\mathbf{4}^{2+}$ and $\mathbf{6}^{2+}$, respectively. Also, for *cis*-β-methylstyrene selectivities above 80% are obtained for $\mathbf{2a}^{2+}$ and $\mathbf{2b}^{2+}$ (entries 2 and 6), while for $\mathbf{4}^{2+}$ and $\mathbf{6}^{2+}$ they are below 60% and 70%, respectively (entries 10 and 14), and for *trans*-stilbene complete conversion and selectivities above 60% are obtained for $\mathbf{2a}^{2+}$ and $\mathbf{2b}^{2+}$ (entries 3 and 7), while for $\mathbf{4}^{2+}$ and $\mathbf{6}^{2+}$ conversion is around 90% and selectivity near 15% (entries 11 and 15). This behaviour can be rationalized on the basis of the electronic nature of the two pairs of complexes. Thus, while for $\mathbf{2a}^{2+}$/$\mathbf{2b}^{2+}$ bi-electronic transfers between the Ru(II) and Ru(IV) species are thermodynamically almost as favourable as the mono-electronic

processes (Ru(III) stability region is minimal with regards to its disproportionation, Fig. 8a and S20), for $\mathbf{4}^{2+}/\mathbf{6}^{2+}$ clearly mono-electronic processes take place (Fig. 8b-c). It is well known that catalysts favouring bi-electronic processes drive epoxidation reactions to concerted pathways and mono-electronic ones drive them to radical mechanisms, the latters usually ending up reducing the selectivity of the whole process by the generation of a wide set of by-products (Scheme S3). [8,15b, 31] Therefore, the existence of bi-electronic processes for $\mathbf{2a}^{2+}/\mathbf{2b}^{2+}$ could explain the higher selectivity observed with regards to their mono-electronic counterparts $\mathbf{4}^{2+}$ and $\mathbf{6}^{2+}$. Also, together with these electronic arguments, other conceivable reasons for the reduced epoxidation capacity of $\mathbf{4}^{2+}/\mathbf{6}^{2+}$ may arise from the chemical nature of their facial ligands, since tpm and bpea are prone to be oxidized under oxidative conditions (they posses aliphatic C atoms), and their steric bulkiness may also difficult the interaction between the substrates and the catalyst active site. Interestingly, different results have been obtained with related Ru-N_5C complexes containing the same auxiliary trpy or bpea ligands but the smaller NHC ligand N-methyl-N'-2-pyridylimidazolium, where the bpea-containing complex yields higher selectivity in front of styrene and higher conversion efficiency and selectivity towards *trans*-stilbene than its corresponding trpy-complex.[15b] Therefore, these results demonstrate again the dramatic influence of the electronic and steric properties of the carbene ligand on the catalytic performance of the Ru complexes.

Table 2 also shows that the studied aqua complexes perform much better with substrates containing electron-donor groups than with those bearing electron-withdrawing substituents, indicating the strong electrophilic character of the Ru^{IV}=O group in all cases. Therefore, the best results are gathered for cyclooctene (entries 4, 8, 12 and 16) whereas the poorest values are obtained for styrene (entries 1, 5, 9 and 13) and *trans*-stilbene (entries 3, 7, 11 and 15), the latter also suffering from potential steric effects due to the bulkiness of its two phenyl rings.

Finally, another interesting feature observed is the stereospecific nature of the catalytic epoxidation process. For the whole set of aqua complexes when *cis*-β-methylstyrene is employed as substrate no *cis*/*trans* isomerization takes place. Therefore, for $\mathbf{4}^{2+}/\mathbf{6}^{2+}$ ring closure must be faster than C-C rotation for the radical intermediates proposed to be formed (Scheme S3, top), while for $\mathbf{2a}^{2+}/\mathbf{2b}^{2+}$ the stereospecificity could be explained on the basis of the proposed concerted bi-electronic oxene insertion to the double bond (Scheme S3, bottom).

Conclusions

A new tetradentate NHC ligand has been synthesized and fully characterized by NMR and X-ray diffraction analysis. This ligand decomposes in nucleophilic solvents at high temperatures due to C-N bond cleavage, generating a bidentate NHC-phtalazine scaffold (PhthaPz-R) during the synthesis of the corresponding four Ru chloro and aqua complexes $[Ru(PhthaPz\text{-}R)(T)X]^{n+}$ (X = Cl, n = 1, X = H_2O, n = 2 ; R = Me, iPr; T = trpy, tpm, bpea), which have been fully characterized electronically and spectroscopically.

Modulation of the thermodynamic stability in aqueous media of the Ru(III) oxidation state has been observed for the four aqua compounds. Thus, while for $\mathbf{4}^{2+}/\mathbf{6}^{2+}$ (T = tpm/bpea) the Ru(III) state is clearly stable at moderately high potentials and they increase their oxidation state from Ru(II) through mono-electronic processes ($\Delta E_{1/2}$ = 200 mV for the latter), for the trpy-based complexes $\mathbf{2a}^{2+}/\mathbf{2b}^{2+}$ the Ru(III) state is almost unstable with regards to its disproportion ($\Delta E_{1/2}$ = 30 mV). This divergence in the electronic behaviour has direct implications in the epoxidation capacity of alkenes with $PhI(OAc)_2$, since the higher conversion and selectivity observed for $\mathbf{2a}^{2+}/\mathbf{2b}^{2+}$ can be rationalized on the basis of the existence of bi-electronic transfers that avoid the generation of radical intermediates of high energy that could reduce the selectivity of the whole process. Additionally, the absence of *cis*/*trans* isomerization in all cases -therefore leading to stereospecific epoxidation processes- may be explained on the basis of either a concerted bi-electronic process ($\mathbf{2a}^{2+}/\mathbf{2b}^{2+}$) or a radical mechanism in which the ring closure is much faster than C-C rotation ($\mathbf{4}^{2+}/\mathbf{6}^{2+}$). Finally, $\mathbf{6}^{2+}$ is by far the most efficient electrocatalyst for the epoxidation of *cis*-β-methylstyrene.

We have also shown that the four aqua complexes are moderately unstable during catalytic water oxidation triggered by Ce(IV) addition due to ligand oxidation under the harsh conditions employed, especially those containing aliphatic carbon atoms ($\mathbf{4}^{2+}/\mathbf{6}^{2+}$). Also, under electrochemically triggered conditions $\mathbf{2a}^{2+}$ is the fastest catalyst at pH 1.0.

In conclusion, in this work we have evidenced that it is possible to modulate the electronic and catalytic properties of Ru NHC complexes by using different auxiliary meridional or facial N-tridentate ligands.

Experimental section

Materials and instrumentation. All reagents used in the present work were obtained from Sigma Aldrich Chemical Co. and were used without further purification. Reagent-grade organic solvents were obtained from Scharlab. $RuCl_3 \cdot 3H_2O$ was supplied by Alfa Aesar. The starting ligands tri(1H-pyrazol-1-yl)methane (tpm) and N,N-bis(pyridin-2-ylmethyl)ethanamine (bpea) were prepared as described in the literature.[32,33] The synthetic manipulations were routinely performed under nitrogen atmosphere using Schlenk flask and vacuum-line techniques.

UV-vis spectroscopy was carried out by a HP8453 spectrometer using 1 cm quartz cells. NMR spectroscopy was performed on a Bruker DPX 250 MHz, DPX 360 MHz, DPX 400 MHz, DPX 500 MHz or a DPX 600 MHz spectrometer. Samples were run in MeOD, DCM-d_2 or acetone-d_6 with internal references. Elemental analyses were performed using a Carlo Erba CHMS EA-1108 instrument from the Chemical Analysis Service of the Universitat Autònoma de Barcelona (SAQ-UAB). Electrospray ionization Mass Spectrometry (ESI-MS) experiments were performed on a HP298s gas chromatography (GC-MS) system from the SAQ-UAB. Cyclic voltammetry and differential pulse voltammetry experiments were performed on the Bio Logic Science Instrument SP-150 potentiostat using a three-electrode cell. A glassy carbon electrode (7 mm diameter) was employed as the working electrode while platinum wire as the auxiliary electrode and a SCE as the reference electrode.

Working electrodes were polished with 0.05 micron Alumina paste and washed with distilled water and acetone before each measurement. The complexes were dissolved in acetonitrile, methanol or dichloromethane solutions of 0.1 M ionic strength containing the necessary amount of n-Bu_4NPF_6 (TABH) as supporting electrolyte. For the electrochemical analysis performed in water, the complexes were dissolved in pH 1 triflic acid solution or solutions of phosphate buffer for other pHs, with a 0.1 M ionic strength. The pH values were increased or reduced by adding drops of a 0.1 M NaOH solution or the pH 1 triflic acid solution. $E_{1/2}$ values here presented were estimated from CV experiments from the average of the oxidative and reductive peak potentials ($E_{p,a}$ + $E_{p,c}$)/2. The electrocatalysis of alkene epoxidation was carried out in dichloromethane (0.1M $TBAPF_6$) at increasing concentrations of *cis*-β-methylstyrene with a glassy carbon as the working electrode and Hg/Hg_2SO_4 as the reference electrode. The CVs were recorded at a scan rate of 100 mV/s. For the epoxidation catalytic studies, experiments were performed as follows. First, a mixing period of 120 min was carried out by adding in a vial 1 mL of 1,2-dichloroethane (DCE) as solvent, 1.60 g (5.0 mmol) of (diacetoxyiodo)benzene ($PhI(OAc)_2$) as oxidant, 1 mmol of 1,1'-biphenyl as internal standard, $2.5\cdot10^{-3}$ mmol of catalyst (**2a**$^{2+}$ to **6**$^{2+}$) and 90 µL (5.0 mmol) of water. This mixing period before substrate addition was observed to be key in order to improve the rate of the catalytic reaction. Then, the substrate (2.5 mmol) was added to the previous mixture, achieving a final volume of approx. 1.47 mL and the corresponding initial concentrations: catalyst, 1.7 mM; substrate, 1.7 M; biphenyl, 0.68 M; $PhI(OAc)_2$, 3.4 M; water, 3.4 M. These concentrations correspond to a catalyst:substrate:oxidant:water ratio of 1:1000:2000:2000. Aliquots were taken every 5, 10, 15, 20, 25 or 30 min until completion of reaction. Each aliquot was filtered through a Pasteur pipette filled with celite; after that diethyl ether was added in order to elute the organic compounds and the filtrate was analyzed in an HP 5890 PACKARD SERIES II Gas Chromatograph (GC) coupled to a mass selective detector with ionization by electronic impact. The characterization of the reaction products was done by comparison with commercial products or by GC-MS spectrometry. GC conditions: initial temperature 40 °C for 10 min, ramp rate variable for each substrate (typically from 10 °C/min to 20 °/min), final temperature 250 °C, injection temperature 220 °C, detector temperature 250 °C. Yield of epoxide and substrate conversion were calculated with regard to the initial concentration of substrate.

Substrate conversion = {$[substrate]_{initial}$ - $[substrate]_{final}$}/$[substrate]_{initial}$·100. Epoxide selectivity = $[epoxide]_{final}$/{$[substrate]_{initial}$-$[substrate]_{final}$}·100.

On-line manometry measurements were performed on a Testo 521 differential pressure manometer with an operating range of 1 to 100 hPa and a measurement accuracy of 0.5%, coupled to thermostatted reaction vessels for dynamic monitoring of the headspace pressure above each reaction. On-line monitoring of the gas evolution was carried out on a Pfeiffer Omnistar GSD 301C mass spectrometer. Typically, a degassed vial of 16.04 mL containing 1.5 mL of a 1.33 mM solution of the catalysts in 0.1 M triflic acid was connected to the apparatus capillary tubing. Subsequently, 0.5 mL of an Ar degassed solution of $(NH_4)_2Ce^{IV}(NO_3)_6$ 400 mM in 0.1 M triflic acid (100 equiv.) were injected by a Hamilton gastight syringe, and the reaction was dynamically monitored at 25 °C. A response ratio of 1:2 was observed when equal concentrations of dioxygen and carbon dioxide were injected, which was used for the calculation of their relative concentrations.

X-ray Crystal Structure Determination. Crystals of **L1**$^{2+}$ were grown by slow diffusion of diethyl ether into a solution of **L1**$(PF_6)_2$ in acetone. Crystals of **5**$^{+}$ were prepared by slow diffusion of diethyl ether into a solution of **5**$^{+}$ in methanol.

Structure solution and refinement was performed using SHELXTL . The crystal data parameters of **L1**$^{2+}$ and **5**$^{+}$ are listed in Table S1 and S2. The structures of **L1**$^{2+}$ and **5**$^{+}$ were analyzed using the programs ORTEP and Mercury.

Synthetic Preparations.

*1,4-bis(1-methylimidazolium-1-yl)phthalazine dichloride (**L1**$(Cl)_2$)*: To an evacuated Schlenk flask a mixture of 1,4-dichlorophthalazine (dcp) (990 mg, 0.5 mol) and 1-methylimidazole (2.050 g 3 mol) were dissolved into 2 ml of DMF. The mixture was stirred under a nitrogen atmosphere at 120°C for 4 hours. A white precipitate appeared in the reaction crude, which was filtered off, washed with DMF and diethyl ether and dried under vacuum. Yield: 1.26 g (70%). ^{1}H-NMR (600 MHz, acetone-d_6, 298K) δ=9.95 (s, 2H, H6, H6'), 8.57 (dd, 2H, $J_{9\text{-}10}$ = 6.2, 3.0 Hz, H9, H9'), 8.50 (s, 2H, H4, H4'), 8.46 (dd, 2H, $J_{10\text{-}9}$ = 6.3, 3.0 Hz, H10, H10'), 8.23 (s, 2H, H3, H3'), 4.39 (m, 6H, H1). ^{13}C-NMR (151 MHz, acetone-d_6, 298K) δ=150.65 (C7), 138.44 (C6), 136.50 (C10), 125.28 (C3), 124.16 (C9), 124.08 (C8), 123.57 (C4), 36.84 (C1). Elemental analysis (% found): C, 52.98; H, 4.49; N, 23.09. Calcd for $C_{16}H_{16}Cl_2N_6$: C, 52.90; H, 4.44; N, 23.14.

cis-[Ru^{II}(PhthaPz-OMe)(trpy)Cl]PF_6 (***1a**(PF$_6$)*): [Ru(trpy)Cl_3] (130 mg, 0.3 mmol), 1,4-bis(1-methylimidazolium-1-yl)phthalazine dichloride (L**1**$(Cl)_2$) (73 mg, 0.2 mmol) and LiCl (38 mg 0.9 mmol) were mixed in a round bottom flask and dry methanol (20 mL) was added as solvent. Triethylamine (121 mg, 166 µL, 1.2 mmol) was added to the solution and the mixture was refluxed at 65°C for 16 hours. After cooling to room temperature, the reaction crude was filtered through celite® to remove the black solid formed and then 20 drops of saturated NH_4PF_6 aqueous solution were added to the filtrate. The solution was concentrated under vacuum until about 10 mL, when a brown precipitate appeared. The precipitate was filtered off, washed with diethyl ether and dried under vacuum. Yield: 62 mg (41%). ^{1}H-NMR (600 MHz, CD_2Cl_2, 298K) δ=8.63 (d, 1H, $J_{4\text{-}3}$ = 2.4 Hz, H4), 8.53 (d, 1H, $J_{9\text{-}10}$ = 8.7 Hz, H9), 8.37 (d, 2H, $J_{26\text{-}27}$ = 8.1 Hz, H26), 8.22 (d, 2H, $J_{23\text{-}22}$ = 8.0 Hz, H23), 8.18 (t, 1H, $J_{27\text{-}26,26'}$ = 8.1 Hz, H27), 8.12 (d, 1H, $J_{12\text{-}11}$ = 8.1 Hz, H12), 8.07 (td, 1H, $J_{10\text{-}9,11}$ = 7.8 Hz, $J_{10\text{-}12}$ = 1.1 Hz, H10), 7.94 (d, 2H, $J_{20\text{-}21}$ = 5.3 Hz, H20), 7.85 (t, 1H, $J_{11\text{-}10,12}$ = 7.6 Hz, H11), 7.82 (t, 2H $J_{22\text{-}21,23}$ = 7.8 Hz, H22), 7.69 (d, 1H $J_{3\text{-}4}$ = 2.4 Hz, H3), 7.20 (td, 2H , $J_{21\text{-}20,22}$ = 6.5 Hz, $J_{21\text{-}23}$ = 1.1 Hz, H21), 4.78 (s, 3H, H1), 3.47 (s, 3H, H18). ^{13}C-NMR (151 MHz, CD_2Cl_2, 298K) 200.66 (C6), 158.75 (C24), 158.43 (C14), 156.51 (C20), 155.50 (C25),

151.45 (C7), 136.59 (C22), 135.43 (C27), 133.91 (C10), 132.29 (C11), 126.88 (C21), 125.83 (C3), 124.51 (C12), 122.95 (C23), 121.16 (C26), 121.00 (C8), 120.20 (C9), 119.51 (C13), 118.77 (C4), 54.61 (C18), 38.15 (C1). UV/vis (methanol): λ_{max}, nm (ε, $M^{-1}\cdot cm^{-1}$)= 281 (11988), 313 (14247), 413 (4700), 475 (4332). ESI-MS (MeOH): m/z = 610.1 ([M-PF_6-1]). Elemental analysis (% found): C, 44.58; H, 3.10; N, 12.95. Calcd for $C_{28}H_{23}ClF_6N_7OPRu$: C, 44.54; H, 3.07; N, 12.99.

cis-[Ru^{II}(PhthaPz-OiPr)(trpy)Cl]PF_6 (***1b***(PF_6)): [Ru(trpy)Cl_3] (130 mg, 0.3 mmol), 1,4-bis(1-methylimidazolium-1-yl)phthalazine dichloride (L**1**$(Cl)_2$) (73 mg, 0.2 mmol) and LiCl (38 mg 0.9 mmol) were mixed in a round bottom flask and dry isopropanol (20 mL) was added as solvent. Triethylamine (121 mg, 166 µL, 1.2 mmol) was added to the solution and the mixture was refluxed at 83°C for 16 hours. After cooling to room temperature, the reaction crude was filtered through celite® to remove the black solid formed and 20 drops of saturated aqueous NH_4PF_6 were added to the filtrate. The solvent was then totally removed in a rotary evaporator and the brown solid obtained was redissolved in isopropanol. The mixture was filtered through celite® and isopropanol was removed from the filtrate under vacuum until about 10 mL left. During this process a brown precipitate appeared, which was filtered off, washed with diethyl ether and dried under vacuum. Yield: 55 mg (35%). ^{1}H-NMR (600 MHz, acetone-d_6, 298K) δ=9.02 (d, 1H $J_{4\text{-}3}$ = 2.4 Hz, H4), 8.84 (d, 1H, $J_{9\text{-}10}$ = 9.0 Hz, H9), 8.75 (d, 2H, $J_{27\text{-}28}$ = 8.1 Hz, H27), 8.57 (d, 2H, $J_{24\text{-}23}$ = 15.8 Hz, H24), 8.35 (t, 1H, $J_{28\text{-}27,27'}$ = 8.1 Hz, H28), 8.11 (m, 4H, $J_{21\text{-}22}$ = 7.2 Hz, H21; $J_{12\text{-}11}$ = 4.8 Hz, H12; $J_{10\text{-}9,11}$ = 9.0 Hz, H10), 8.00 (d, 1H, $J_{3\text{-}4}$ = 2.4 Hz, H3), 7.92 (m, 3H, H11, H23), 7.29 (ddd, 1H, $J_{22\text{-}21,23,24}$ = 7.0, 5.6, 1.2 Hz, H22), 4.79 (s, 3H, H1), 4.54 (sept, 1H, $J_{18\text{-}19}$ = 6.2 Hz, H18), 1.09 (d, 1H, $J_{19\text{-}18}$ = 6.2 Hz, H19). ^{13}C-NMR (151 MHz, acetone-d_6, 298K) 200.91 (C6), 159.08 (C25), 157.41 (C14), 156.82 (C21), 155.61 (C26), 151.44 (C7), 136.70 (C23), 135.48 (C28), 133.82 (C10), 132.09 (C11), 126.85 (C22), 126.03 (C3), 124.30 (C12), 123.13 (C24), 121.64 (C27), 121.28 (C8), 120.94 (C9), 119.61 (C13), 119.14 (C4), 70.79 (C18), 37.48 (C1), 20.96 (C19). UV/vis (methanol): λ_{max}, nm (ε, $M^{-1}\cdot cm^{-1}$)= 276 (11315), 314 (14616), 413 (5036), 479 (3889). ESI-MS (MeOH): m/z = 638.1 ([M-PF_6-1]). Elemental analysis (% found): C, 46.07; H, 3.52; N, 12.49. Calcd for $C_{30}H_{27}ClF_6N_7OPRu$: C, 46.01; H, 3.48; N, 12.52.

[Ru^{II}(PhthaPz-OMe)(tpm)Cl]PF_6 (***3***(PF_6)): [Ru(tpm)Cl_3] (130 mg, 0.3 mmol), 1,4-bis (1-methylimidazolium-1-yl)phthalazine dichloride (L**1**$(Cl)_2$) (73 mg, 0.2 mmol) and LiCl (38 mg 0.9 mmol) were mixed in a round bottom flask and dry methanol (20 mL) was added as solvent. Triethylamine (121 mg, 166 µL, 1.2 mmol) was added to the solution and the mixture was refluxed at 65°C for 16 hours. After cooling to room temperature, the reaction crude was filtered through celite® to remove the black solid formed and 20 drops of saturated aqueous NH_4PF_6 were added to the filtrate. The methanolic solution was concentrated in a rotary evaporator until about 10 mL and a brown precipitate was obtained. The precipitate was filtered off, washed with diethyl ether and dried under vacuum. Yield: 88 mg (60%). ^{1}H-NMR (600 MHz, acetone-d_6, 298K) δ=9.66 (s, 1H, H24), 8.88 (d, 1H, $J_{4\text{-}3}$ = 2.3 Hz, H4), 8.87 (d, 1H, $J_{9\text{-}10}$ = 8.6 Hz, H9), 8.68 (d, 1H, $J_{20\text{-}21}$ = 1.6 Hz, H20), 8.57 (d, 1H, $J_{31\text{-}32}$ = 2.3 Hz, H31), 8.52 (d, 1H, $J_{22\text{-}21}$ = 2.2 Hz, H22), 8.47 (d, 1H, $J_{33\text{-}32}$ = 1.7 Hz, H33), 8.46 (d, 1H, $J_{26\text{-}27}$ = 2.5 Hz, H26), 8.39 (d, 1H, $J_{12\text{-}11}$ = 8.0 Hz, H12), 8.20 (t, 1H, $J_{10\text{-}9,11}$ = 7.3 Hz, H10), 8.07 (t, 1H, $J_{11\text{-}10,12}$ = 7.6 Hz, H11), 7.64 (d, 1H, $J_{3\text{-}4}$ = 2.3 Hz, H3), 6.89 (d, 1H, $J_{28\text{-}27}$ = 1.9 Hz, H28), 6.74 (t, 1H, $J_{21\text{-}20,22}$ = 2.3 Hz, H21), 6.67 (t, 1H, $J_{32\text{-}31,33}$ = 2.4 Hz, H32), 6.33 (t, 1H, $J_{27\text{-}26,28}$ = 2.4 Hz, H27), 4.16 (s, 3H, H18), 3.73 (s, 3H, H1). ^{13}C-NMR (151 MHz, acetone-d_6, 298K) 205.44 (C6), 157.87 (C14), 151.40 (C7), 149.12 (C33), 146.71 (C28), 146.66 (C20), 134.70 (C26), 133.97 (C31), 133.75 (C10), 132.43 (C22), 132.27 (C11), 124.89 (C3), 124.34 (C12), 121.57 (C8), 121.28 (C9), 120.17 (C13), 119.63 (C4), 108.41 (C32), 108.27 (C27), 107.51 (C21), 76.77 (C24), 55.04 (C18), 36.27 (C1). UV/vis (methanol): λ_{max}, nm (ε, $M^{-1}\cdot cm^{-1}$)= 302 (7799), 410 (4745). ESI-MS (MeOH): m/z = 591.1 ([M-PF_6-1]). Elemental analysis (% found): C, 37.60; H, 3.05; N, 18.99. Calcd for $C_{23}H_{22}ClF_6N_{10}OPRu$: C, 37.53; H, 3.01; N, 19.03.

trans,fac-[Ru^{II}(PhthaPz-OMe)(bpea)Cl]PF_6 (***5***(PF_6)): [Ru(bpea)Cl_3] (130 mg, 0.3 mmol), 1,4-bis(1-methylimidazolium-1-yl)phthalazine dichloride (L**1**$(Cl)_2$) (73 mg, 0.2 mmol) and LiCl (38 mg 0.9 mmol) were mixed in a round bottom flask and dry methanol (20 mL) was added as solvent. Triethylamine (121 mg, 166 µL, 1.2 mmol) was added to the solution and the mixture was refluxed at 65°C for 16 hours. After cooling to room temperature, the reaction crude was filtered through celite® to remove the black solid formed and 20 drops of saturated aqueous NH_4PF_6 were added to the filtrate. The methanolic solution was concentrated in a rotary evaporator until about 10 mL left and a brown precipitate appeared. The precipitate was filtered, washed with diethyl ether and dried under vacuum. Yield: 68 mg (45%). ^{1}H-NMR (600 MHz, acetone-d_6, 298K) δ=9.63 (d, 1H, $J_{20\text{-}21}$ = 5.3 Hz, H20), 9.56 (d, 1H, $J_{34\text{-}33}$ = 5.0 Hz, H34), 8.84 (d, 1H, $J_{4\text{-}3}$ = 2.0 Hz, H4), 8.79 (d, 1H, $J_{9\text{-}10}$ = 8.3 Hz, H9), 8.25 (d, 1H, $J_{12\text{-}11}$ = 8.0 Hz, H12), 8.12 (t, 1H, $J_{10\text{-}9,11}$ = 7.5 Hz, H10), 7.97 (t, 1H, $J_{11\text{-}10,12}$ = 7.6 Hz, H11), 7.92 (t, 1H, $J_{32\text{-}31,33}$ = 7.3 Hz, H32), 7.82 (t, 1H, $J_{22\text{-}21,23}$ = 7.4 Hz, H22), 7.58 (m, 2H, $J_{3\text{-}4}$ = 2.3 Hz, $J_{31\text{-}32}$ = 7.3 Hz, H3, H31), 7.50 (m, 1H, $J_{23\text{-}22,33\text{-}32,34}$ = 7.3 Hz, H23, H33), 7.41 (t, 1H, $J_{21\text{-}20,22}$ = 6.5 Hz, H21), 4.52-4.42 (m, 4H, H25, H29) 3.65 (s, 3H, H18), 3.58 (s, 3H, H1), 2.53 (m, 1H, $J_{27\text{-}27',28}$ = 13.8, 6.8 Hz, H27), 2.35 (m, 1H, $J_{27'\text{-}27,28}$ = 13.7, 6.8 Hz, H27'), 0.91 (m, 3H, H28). ^{13}C-NMR (151 MHz, acetone-d_6, 298K) 204.97 (C6), 161.42 (C20), 160.02 (C34), 158.07 (C14), 151.65 (C24), 150.15 (C13), 149.42 (C30), 136.55 (C32), 125.73 (C22), 133.74 (C10), 131.47 (C11), 125.00 (C3), 124.30 (C12), 123.63 (C21), 123.13 (C33), 121.52 (C8), 121.01 (C23), 120.70 (C9), 120.64 (C31), 119.44 (C7), 118.85 (C4), 67.49 (C25), 66.09 (C29), 61.96 (C27), 53.89 (C18), 35.45 (C1), 7.98 (C28). UV/vis (methanol): λ_{max}, nm (ε, $M^{-1}\cdot cm^{-1}$)= 299 (5226), 434 (5612). ESI-MS (MeOH): m/z = 604.1 ([M-PF_6-1]). Elemental analysis (% found): C, 43.37; H, 3.94; N, 13.05. Calcd for $C_{27}H_{29}ClF_6N_7OPRu$: C, 43.29; H, 3.90; N, 13.09.

cis-[Ru^{II}(PhthaPz-OMe)(trpy)(OH$_2$)](PF$_6$)$_2$ (***2a***$(PF_6)_2$): **1a**$^+$ (120 mg, 0.16 mmol) was dissolved in a mixture of acetone and water (acetone: water = 1: 3, 40 mL). $AgBF_4$ (109 mg, 0.56 mmol) was added into the solution, which was then refluxed at 90°C for 4 hours. After cooling to room temperature, the reaction crude was filtered through celite® to remove the black solid formed. The red-brown solution was concentrated under vacuum until about 20 mL left, followed by centrifugation (10000rpm, 10min) to remove the potential colloidal silver still remaining. To the clear red solution 20

drops of saturated aqueous NH_4PF_6 solution were added and the precipitate formed was filtered off, washed with diethylether and dried under vacuum. Yield: 91 mg (65%). ^{1}H-NMR (600 MHz, acetone-d_6, 298K) 9.01 (d, 1H, $J_{4\text{-}3}$ = 2.4 Hz, H4), 8.80 (d, 2H, $J_{26\text{-}27}$ = 7.4 Hz, H26), 8.78 (d, $J_{9\text{-}10}$ = 8.7 Hz, H9), 8.62 (d, 2H, $J_{23\text{-}22}$ = 8.0 Hz, H23), 8.44 (t, 2H, $J_{27\text{-}26,26'}$ = 8.1 Hz, H27), 8.19 (d, 2H, $J_{20\text{-}21}$ = 5.0 Hz, H20), 8.12 (t, 1H, $J_{10\text{-}9,11}$ = 8.7 Hz, H10), 8.04-8.00 (m, 4H, H12, H3, H22), 7.91 (t, 1H, $J_{11\text{-}10,12}$ = 7.5 Hz, H11), 7.37 (m, 2H, H21), 4.56 (s, 3H, H1), 3.46 (s, 3H, H18). ^{13}C-NMR (151 MHz, acetone-d_6, 298K) 200.62 (C6), 159.47 (C24), 158.01 (C14), 157.82 (C20), 156.41 (C25), 153.08 (C7), 138.22 (C22), 137.65 (C27), 134.20 (C10), 132.83 (C11), 127.53 (C21), 126.29 (C3), 124.05 (C12), 123.85 (C23), 122.38 (C26), 121.12 (C9), 120.90 (C8), 119.57 (C14), 119.21 (C3), 54.43 (C18), 36.55 (C1). UV/vis (methanol): λ_{max}, nm (ε, $M^{-1}\cdot cm^{-1}$)= 275 (12189), 309 (13040), 388 (4338), 467 (4474). ESI-MS (MeOH): m/z = 594.1 ([M-2PF_6]). Elemental analysis (% found): C, 38.14; H, 2.89; N, 11.06. Calcd for $C_{28}H_{25}F_{12}N_7O_2P_2Ru$: C, 38.11; H, 2.86; N, 11.11.

cis-[Ru^{II}(PhthaPz-OiPr)(trpy)(OH$_2$)](PF$_6$)$_2$ (***2b***(PF$_6$)$_2$): **1b**$^+$ (120mg, 0.15 mmol) was dissolved in a 40 mL mixture of acetone and water (1:3). $AgBF_4$ (109 mg, 0.56 mmol) was then added to the solution, which was then refluxed at 90°C for 4 hours. After cooling to room temperature, the reaction crude was filtered through celite® to remove the silver chloride formed. The brown filtrate was then concentrated in a rotary evaporator until about 20 mL, followed by centrifugation (10000 rpm, 10 min) to remove the remaining solids. To the clear red solution 20 drops of a saturated aqueous NH_4PF_6 solution were added. The brown precipitate formed was filtered off, washed with diethyl ether and dried under vacuum. Yield: 91 mg (65%). ^{1}H-NMR (600 MHz, acetone-d_6, 298K) δ=9.03 (d, 1H, $J_{4\text{-}3}$ = 2.4 Hz, H4), 8.84 (d, 2H, $J_{27\text{-}28}$ = 6.7 Hz, H27), 8.81 (d, 1H, $J_{9\text{-}10}$ = 8.7 Hz, H9), 8.63 (d, 2H, $J_{24\text{-}23}$ = 8.0 Hz, H24), 8.50 (t, 1H, $J_{28\text{-}27,27'}$ = 8.1 Hz, H28), 8.23 (dd, 2H, $J_{21\text{-}22,23}$ = 10.5, 5.6 Hz, H21), 8.13 (t, 1H, $J_{10\text{-}9,11}$ = 8.5, Hz, H10), 8.10 (d, 1H, $J_{12\text{-}11}$ = 8.7 Hz, H12), 8.06-8.01 (m, 3H, H3, H23), 7.93 (t, 1H, $J_{11\text{-}10,12}$ = 7.6 Hz, H11), 7.38 (ddd, 1H, $J_{22\text{-}21,23,24}$ = 7.0, 5.6, 1.2 Hz, H22), 4.58 (s, 3H, H1), 4.49 (dt, 1H, $J_{18\text{-}19,19'}$ = 12.3, 6.2 Hz, H18), 1.07 (d, 6H, $J_{19\text{-}18}$ = 6.2 Hz, H19). ^{13}C-NMR (151 MHz, acetone-d_6, 298K) 200.66 (C6), 159.47 (C25), 157.96 (C21), 157.31 (C14), 156.32 (C26), 152.73 (C7), 138.23 (C23), 137.53 (C28), 134.05 (C10), 132.74 (C11), 127.63 (C22), 126.16 (C3), 124.24 (C12), 123.77 (C24), 122.47 (C27), 121.15 (C8), 121.07 (C9), 119.80 (C13), 119.62 (C4), 70.98 (C18), 36.39 (C1), 20.90 (C19). UV/vis (methanol): λ_{max}, nm (ε, $M^{-1}\cdot cm^{-1}$)= 280 (12006), 311 (14895), 392 (4700), 463 (4220). ESI-MS (MeOH): m/z = 622.1 ([M-2PF_6]). Elemental analysis (% found): C, 39.63; H, 3.24; N, 10.74. Calcd for $C_{30}H_{29}F_{12}N_7O_2P_2Ru$: C, 39.57; H, 3.21; N, 10.77.

[Ru^{II}(PhthaPz-OMe)(tpm)(OH$_2$)](PF$_6$)$_2$ (***4***(PF$_6$)$_2$): **3**$^+$ (120 mg, 0.16 mmol) was dissolved in a 40 mL mixture of acetone and water (1:3). $AgBF_4$ (109 mg, 0.56 mmol) was added into the solution that was then refluxed at 90°C for 4 hours. After cooling to room temperature, the reaction crude was filtered through celite® to remove the silver chloride formed. The brown filtrate was then concentrated in a rotary evaporator until about 20 mL, followed by centrifugation (10000 rpm, 10 min) in order to remove the remaining solids. To the clear red solution 20 drops of a saturated aqueous NH_4PF_6 solution were added. The red precipitate formed was filtered off, washed with diethyl ether and dried under vacuum. Yield: 76 mg (55%). ^{1}H-NMR (600 MHz, acetone-d_6, 298K) δ=9.90 (s, 1H, H24), 8.99 (d, 1H, $J_{4\text{-}3}$ = 2.4 Hz, H4), 8.97 (d, 1H, $J_{9\text{-}10}$ = 8.5 Hz, H9), 8.83 (d, 1H, $J_{20\text{-}21}$ = 1.7 Hz, H20), 8.72 (d, 1H, $J_{31\text{-}32}$ = 2.9 Hz, H31), 8.67 (d, 1H, $J_{22\text{-}21}$ = 2.7 Hz, H22), 8.58 (d, 1H, $J_{33\text{-}32}$ =2.0 Hz, H33), 8.53 (d, 1H, $J_{26\text{-}27}$ = 5.5 Hz, H26), 8.47 (d, 1H, $J_{12\text{-}11}$ = 8.1 Hz, H12), 8.29 (dd, 1H, $J_{10\text{-}9,11}$ = 8.2, 7.7 Hz, H10), 8.17 (t, 1H, $J_{11\text{-}10,12}$ = 7.7 Hz, H11), 7.74 (d, 1H, $J_{3\text{-}4}$ = 2.3 Hz, H3), 6.85 (m, $J_{21\text{-}20,22}$ = 2.4 Hz, $J_{28\text{-}27}$ = 2.2 Hz, H21, H28), 6.80 (t, 1H, $J_{32\text{-}31,33}$ = 2.5 Hz, H32), 6.34 (t, 1H, $J_{27\text{-}26,28}$ = 2.5 Hz, H27), 4.20 (s, 3H, H18), 3.74 (s, 1H, H1). ^{13}C-NMR (151 MHz, acetone-d_6, 298K) 200.22 (C6), 158.58 (C14), 152.76 (C7), 148.70 (C33), 148.04 (C28), 147.06 (C20), 135.74 (C26), 134.89 (C31), 134.17 (C10), 133.64 (C22), 133.40 (C11), 125.84 (C3), 124.48 (C12), 122.02 (C9), 121.75 (C8), 120.96 (C13), 120.61 (C4), 109.06 (C32), 108.69 (C27), 108.04 (C21), 76.61 (C24), 55.38 (C18), 36.65 (C1). UV/vis (methanol): λ_{max}, nm (ε, $M^{-1}\cdot cm^{-1}$)= 295 (8297), 392 (5315). ESI-MS (MeOH): m/z = 575.1 ([M-2PF_6]). Elemental analysis (% found): C, 32.02; H, 2.81; N, 16.19. Calcd for $C_{23}H_{24}F_{12}N_{10}O_2P_2Ru$: C, 31.99; H, 2.80; N, 16.22.

trans,fac-[Ru^{II}(PhthaPz-OMe)(bpea)(OH$_2$)](PF$_6$)$_2$ (***6***(PF$_6$)$_2$): **5**$^+$ (120 mg, 0.16 mmol) was dissolved in a 40 mL mixture of acetone and water (1: 3). $AgBF_4$ (109 mg, 0.56 mmol) was then added into the solution, which was refluxed at 90°C for 4 hours. After cooling to room temperature, the reaction crude was filtered through celite® to remove the silver chloride formed. The red-brown solution was concentrated in a rotary evaporator until about 20 mL, followed by centrifugation (10000 rpm, 10 min) to remove the remaining solids. To the clear red solution 20 drops of a saturated aqueous NH_4PF_6 solution were added. The precipitate formed was filtered off, washed with diethyl ether and dried under vacuum. Yield: 96 mg (68%). ^{1}H-NMR (600 MHz, acetone-d_6, 298K) δ=8.99 (d, 1H, $J_{4\text{-}3}$ = 2.4 Hz, H4), 8.96 (d, 1H, $J_{34\text{-}33}$ = 5.3 Hz, H34), 8.93 (m, 2H, H20, H9), 8.36 (d, 1H, $J_{12\text{-}11}$ = 8.1 Hz, H12), 8.23 (t, 1H, $J_{10\text{-}9,11}$ = 7.7 Hz, H10), 8.08 (t, 1H, $J_{11\text{-}10,12}$ = 7.6 Hz, H11), 7.99 (td, 1H, $J_{32\text{-}33,31}$ = 7.8, $J_{32\text{-}34}$ = 1.4 Hz, H32), 7.88 (td, 1H, $J_{22\text{-}23,21}$ = 7.4, $J_{22\text{-}20}$ = 1.7 Hz, H22), 7.72 (d, 1H, $J_{3\text{-}4}$ = 2.4 Hz, H3), 7.67 (d, 1H, $J_{31\text{-}32}$ = 7.9 Hz, H31), 7.57 (m, 1H, H33), 7.55 (d, 1H, $J_{23\text{-}22}$ = 7.9 Hz, H23), 7.50 (t, 1H, $J_{21\text{-}22,20}$ = 6.6 Hz, H21), 4.57-4.40 (m, 4H, H25, H29), 3.71 (s, 3H, H1), 3.65 (s, 3H, H18), 2.40 (m, 1H, $J_{27\text{-}27',28}$ = 9.2, 5.0 Hz, H27), 2.30 (m, 1H, $J_{27'\text{-}27,28}$ = 9.2, 5.0 Hz, H27'),0.91 (t, 3H, $J_{28\text{-}27,27'}$ = 7.0 Hz, H28). ^{13}C-NMR (151 MHz, acetone-d_6, 298K) 202.85 (C6), 161.20 (C24), 159.56 (C30), 158.81 (C14), 151.85 (C7), 149.37 (C20), 147.67 (C34), 137.42 (C32), 136.72 (C22), 134.06 (C10), 132.67 (C11), 125.82 (C3), 124.41 (C12), 124.30 (C21), 123.78 (C33), 121.63 (C8), 121.54 (C23), 121.49 (C31), 121.35 (C9), 120.47 (C13), 119.89 (C4), 67.89 (C25), 67.29 (C29), 62.80 (C27), 54.19 (C18), 35.89 (C1), 7.97 (C28). UV/vis (methanol): λ_{max}, nm (ε, $M^{-1}\cdot cm^{-1}$)= 299 (5810), 423 (5753). ESI-MS (MeOH): m/z = 586.1 ([M-2PF_6]). Elemental analysis (% found): C, 37.06; H, 3.60; N, 11.15. Calcd for $C_{27}H_{31}F_{12}N_7O_2P_2Ru$: C, 36.99; H, 3.56; N, 11.19.

Acknowledgements

Support form MINECO (CTQ2011-26440 and CTQ2015-64261-R) is gratefully acknowledged. M.G.-S. is grateful for the award of a PIF doctoral grant from UAB.

Notes and references

1 W. A. Herrmann and C. Köcher, *Angew. Chem. Int. Ed.* 1997, **36**, 2162.

2 (*a*) M. N. Hopkinson, C. Richter, M. Schedler and F. Glorious, *Nature* 2014, **510,** 485; (*b*) S. Kaufhold, L. Petermann, R. Staehle and S. Rau, *Coord. Chem. Rev.* 2015, **304-305**, 73.

3 A. Dovletoglou, S. A. Adeyemi and T. J. Meyer, *Inorg. Chem.* 1996, **35**, 4120.

4 (*a*) X. Sala, S. Maji, R. Bofill, J. García-Antón, L. Escriche and A. Llobet, *Acc. Chem. Res.* 2014, **47**, 504; (*b*) M. Dakkach, M. I. López, I. Romero, M. Rodríguez, A. Atlamsan, T. Parella, X. Fontrodona and A. Llobet, *Inorg. Chem.* 2010, **49**, 7072.

JO HI AFEGIRIA UNA HARD-CORE PCET REF D'EN TJM O D'ALTRES

5 (*a*) R. Lalrempuia, N. D. McDaniel, H. Müller-Bunz, S. Bernhard and M. Albrecht, *Angew. Chem. Int. Ed.* 2010, **49**, 9765; (*b*) A. Petronilho, M. Rahman, J. A. Woods, H. Al-Sayyed, H. Müller-Bunz, J. M. Don MacElroy, S. Bernhard and M. Albrecht, *Dalton Trans.* 2012, **41**, 13074; (*c*) A. Petronilho, J. A. Woods, S. Bernhard and M. Albrecht, *Eur. J. Inorg. Chem.* 2014, 708; (*d*) Z. Codolà, J. M. S. Cardoso, B. Royo, M. Costas and J. Lloret-Fillol, *Chem. Eur. J.* 2013, **19**, 7203; (*e*) A. Volpe, A. Sartorel, C. Tubaro, L. Meneghini, M. Di Valentin, C. Graiff and M. Bonchio, *Eur. J. Inorg. Chem.* 2014, 665; (*f*) I. Corbucci, A. Petronilho, H. Müller-Bunz, L. Rocchigiani, M. Albrecht and A. Macchioni, *ACS Catal.* 2015, **5**, 2714.

6 (*a*) Z. Chen, J. J. Concepcion and T. J. Meyer, *Dalton Trans.* 2011, **40**, 3789; (*b*) R. Staehle, L. Tong, L. Wang, L. Duan, A. Fischer, M. S. G. Ahlquist, L. Sun and S. Rau, *Inorg. Chem.* 2014, **53**, 1307.

7 (*a*) L. Francàs, R. Bofill, J. García-Antón, L. Escriche, X. Sala and A. Llobet, *Ru-Based Water Oxidation Catalysts*, in *Molecular Water Oxidation Catalysts: A Key Topic for New Sustainable Energy Conversion Schemes*, ed. A. Llobet, John Wiley & Sons, Ltd, 2014, p. 29-50; (*b*) J. García-Antón, R. Bofill, L. Escriche, A. Llobet and X. Sala, *Eur. J. Inorg. Chem.* 2012, 4775. (c) N. Planas, G. J. Christian, E. Mas-Marza, X. Sala, X. Fontrodona, F. Maseras, A. Llobet, *Chem. Eur. J.* 2010, **16**, 7965-7968. (d) L. Mognon, S. Mandal, C. E. Castillo, J. Fortage, F. Molton, G. Aromi, J. Benet-Buchhlolz, M.-N. Collomb, A. Llobet, *Chem. Sci.*, 2016, ***7***, 3304-3312.

8 (*a*) E. Masllorens, M. Rodríguez, I. Romero, A. Roglans, T. Parella, J. Benet-Buchholz, M. Poyatos and A. Llobet, *J. Am. Chem. Soc.* 2006, **128**, 5306; (*b*) L. Vaquer, P. Miró, X. Sala, F. Bozoglian, E. Masllorens, J. Benet-Bucholz, X. Fontrodona, T. Parella, I. Romero, A. Roglans, M. Rodríguez, C. Bo and A. Llobet , *ChemPlusChem* 2013, **78**, 235.

9 (*a*) F. R. Keene, *Coord. Chem. Rev.* 1999, **187**, 121; (*b*) T. J. Meyer, *J. Electrochem. Soc.* 1984, **131**, 221C.

10 J. Aguiló, A. Naeimi, R. Bofill, H. Mueller-Bunz, A. Llobet, L. Escriche, X. Sala and M. Albrecht, *New. J. Chem.* 2014, **38**, 1980.

11 (*a*) J. Van Veldhuizen, J. Campbell, R. Giudici and A. Hoveyda, *J. Am. Chem. Soc.* 2005, **127**, 6877; (*b*) B. J. Truscott, R. Klein and P. T. Kaye, *Tetrahedron Letters* 2010, **51**, 5041.

12 J. Aguiló, L. Francàs, R. Bofill, M. Gil-Sepulcre, J. García-Antón, A. Poater, A. Llobet, L. Escriche, F. Meyer and X. Sala, *Inorg. Chem.* 2015, **54**, 6782.

13 (*a*) C. Chen, H. Y. Qiu, W. Z. Chen and D. Q. Wang, *J. Organomet. Chem.* 2008, **693**, 3273; (*b*) J. S. Ye, X. M. Zhang, W. Z. Chen and S. Shimada, *Organometallics*, 2008, **27**, 4166; (*c*) X. L. Liu and W. Z. Chen, *Organometallics*, 2012, **31**, 6614.

14 J. Mola, I. Romero, M. Rodríguez, F. Bozoglian, A. Poater, M. Solà, T. Parella, J. Benet-Buchholz, X. Fontrodona and A. Llobet, *Inorg. Chem.* 2007, **46**, 10707.

15 (*a*) M. Dakkach, T. Parella, A. Atlamsani, I. Romero and M. Rodríguez, *Adv. Synth. Catal.* 2011, **353**, 231; (*b*) M. Dakkach, A. Atlamsani, T. Parella, I. Romero and M. Rodríguez, *Inorg. Chem.* 2013, **52**, 5077.

16 L. Vaquer, J. De Tovar, J. García-Antón, A. Llobet and X. Sala, *Inorg. Chem*. 2013, **52**, 4985.

17 (*a*) X. Sala, A. Poater, A. Von Zelewsky, T. Parella, X. Fontrodona, I. Romero, M. Solà, M. Rodríguez and A. Llobet, *Inorg. Chem.* 2008, **47**, 8016; (*b*) J. S. Ye, X. M. Zhang, W. Z. Chen and S. Shimada, *Organometallics*, 2008, **27**, 4166.

18 F. Laurent, E. Plantalech, B. Donnadieu, A. Jiménez, F. Hernández, M. Martínez-Ripoll, M. Biner and A. Llobet, *Polyhedron*, 1999, **18**, 3321.

19 K. J. Takeuchi, M. S. Thompson, D. W. Pipes and T. J. Meyer, *Inorg. Chem.* 1984, **23**, 1845.

20 A. Llobet, P. Doppelt and T. J. Meyer, *Inorg. Chem.* 1988, **27**, 514.

21 M. Rodríguez, I. Romero and A. Llobet, *Inorg. Chem.* 2001, **40**, 4150.

22 (*a*) J. C. Dobson and T. J. Meyer, *Inorg. Chem.* 1988, **27**, 3283; (*b*) G. E. Cabaniss, A. A. Diamantis, W. R. Murphy, R. W. Linton and T. J. Meyer, *J. Am. Chem. Soc.* 1985, **107**, 1845.

23 C. Costentin, S. Drouet, M. Robert and J.-M. Savéant, *J. Am. Chem. Soc.* 2012, **134**, 11235.

24 R. Matheu, S. Neudeck, F. Meyer, X. Sala, A. Llobet, *ChemSusChem* 2016, **xx**, xxxx-xxxx.

25 R. Matheu, M. Z. Ertem, J. Benet-Buchholz, E. Coronado, V. S.

Batista, X. Sala and A. Llobet, *J. Am. Chem. Soc.* 2015, **137**, 10786.
26 E. S. Rountree, B. D. McCarthy, T. T. Eisenhart and J. L. Dempsey, Inorg. Chem. 2014, **53**, 9983.
27 L. Francàs, X. Sala, E. Escudero-Adan, J. Benet-Buchholz, L. Escriche and A. Llobet, *Inorg. Chem.* 2011, **50**, 2771.
28 J. Aguiló, L. Francàs, H. J. Liu, R. Bofill, J. García-Antón, J. Benet-Buchholz, A. Llobet, L. Escriche and X. Sala, *Catal. Sci. Technol.* 2014, **4**,190.
29 A. J. Bard and L. R. Faulkner, *Electrochemical Methods: Fundamentals and Applications* 2nd Edition, John Wiley & Sons, New York, 2001.
30 J.-H. In, S.-E. Park, R. Song and W. Nam, *Inorg. Chim. Acta* 2003, **343**, 373.
31 (*a*) L. K. Stultz, R. A. Binstead, M. S. Reynolds and T. J. Meyer, *J. Am. Chem. Soc.* 1995, **117**, 2520; (*b*) W.-H. Fung, W.-Y. Yu and C.-M. Che, *J. Org. Chem.* 1998, **63**, 7715.
32 D. L. Reger, T. C. Grattan, K. J. Brown, C. A. Little, J. J. S. Lamba, A. L. Rheingold and R. D. Sommer, *J. Organomet. Chem.*, 2000, **607**, 120.
33 S. Pal, M. K. Chan and W. H. Armstrong, *J. Am. Chem. Soc.* 1992, **114**, 6398.

1. Figures 9 i S25 (1. estaria be posar-hi els blancs si els teniu l 2 la conc del inset ha de ser [4] o [2] o [6])